This is the accepted version of our manuscript, revised after peer review and accepted for publication in Pure and Applied Geophysics.

Station-orientation catalog for Australian broadband seismic stations

Kotaro Tarumi[1,2*] and Kazunori Yoshizawa[1,2]

[1*]Department of Natural History Sciences, Graduate School of Science, Hokkaido University, Sapporo, 0600810, Japan.
[2]Department of Earth and Planetary Sciences, Faculty of Science, Hokkaido University, Sapporo, 0600810, Japan.

*Corresponding author(s). E-mail(s): tarumi.kotaro.jp@gmail.com;
Contributing authors: yoshizawa@sci.hokudai.ac.jp;

Abstract

Many broadband seismic stations deployed permanently and temporarily in the Australian continent have been used for various seismological investigations in and around Australia. Although two horizontal components are generally assumed to be oriented in the north and east directions, as reported by data providers, misorientations of horizontal components from the true geographic north direction cannot be avoided in practical field observations, even at well-maintained permanent stations. In this paper, we applied a polarization analysis to almost all stations in Australia to estimate the misorientations of horizontal components using long-period teleseismic P-waves. A large data set of P-wave arrival angles allows us to successfully detect probable horizontal misorientations, including significant temporal changes in some stations, which generally coincide with reported equipment replacements included in the EarthScope (IRIS) catalog. However, we also detected some unreported temporal changes in station orientation that may result from undocumented maintenance activities, such as sensor reorientation, which are typically not reflected in metadata. Improper corrections for orientation may affect waveform-based studies for the Earth's internal exploration, as demonstrated by teleseismic receiver function analyses, especially in the transverse component. Compiling the information on such time-dependent misorientations, we created a full catalog of horizontal-component orientations for both permanent and temporary stations in Australia, which is widely available for the community.

Keywords: Australia, Seismometer misorientation, P-wave polarization, Receiver function

1 Introduction

A large number of broadband seismic stations deployed permanently or temporarily in the Australian continent have provided key information on seismic wave propagation (e.g., Kennett and Furumura, 2008), seismic sources (e.g., Hejrani and Tkalčić, 2020), and seismic structure (e.g., Kennett et al, 2013; Yoshizawa, 2014; Birkey and Ford, 2023; Eakin et al, 2023) in and around Australia. As an initial step for the three-component seismic waveform analysis, we generally rotate two horizontal components (e.g., NS / EW) to radial and transverse directions, supposing that the horizontal sensors are oriented in the north and east (or in reported) directions. However, as several earlier studies suggested, there is a possibility of nontrivial misorientation of horizontal components at some stations (e.g., Laske, 1995; Yoshizawa et al, 1999; Schulte-Pelkum et al, 2001). Also, temporal changes in the amplitude gain of seismometers may occur at some permanent stations over a long observation period (Ekström et al, 2006). Such errors or uncertainties in the documented catalog values, particularly the ambiguities in the horizontal-component orientation, would prevent us from performing precise waveform analyses that depend on the horizontal directions, such as shear-wave splitting measurements, Love-wave dispersion analysis, and the azimuthal dependency of receiver functions.

The horizontal orientation of seismic stations can be estimated by measuring the arrival angles of teleseismic P waves (e.g., Yoshizawa et al, 1999; Schulte-Pelkum et al, 2001; Albuquerque et al, 2024; Deng et al, 2024) or Rayleigh waves (e.g., Laske and Masters, 1996; Larson and Ekström, 2002; Ekström and Busby, 2008) at longer periods for a large number of seismic events. Zha et al (2013) developed the method for determining the horizontal orientation of ocean bottom seismometers based on the vertical-radial cross correlation of Rayleigh-wave polarization from ambient noise data. More recently, Sun et al (2024) developed an alternative method for measuring station orientation using the azimuthal dependence of receiver function amplitudes for the direct P-phase.

Rayleigh waves generally oscillate elliptically in the radial-vertical plane, but their particle motions become more complicated in heterogeneous and anisotropic media (Crampin, 1975). Moreover, due to the dispersive nature of surface waves, the arrival-angle anomalies (or deviations from the great-circle path) depend significantly on the frequency (Laske, 1995; Yoshizawa et al, 1999), which may increase uncertainties in the estimated station orientation. Furthermore, the overlaps by preceding Love waves in the transverse component make it difficult to perform arrival-angle analysis of Rayleigh waves at relatively shorter epicentral distances of less than 50° (Yoshizawa et al, 1999). On the contrary, the onset of teleseismic P-waves exhibits a relatively simple linear motion in the radial-vertical plane without frequency dependence. Teleseismic P waves with the near-vertical incidence to the station mainly sample the lower mantle where lateral heterogeneities are weak. Thus, the ray-bending effects on P-waves due to strong lateral heterogeneity in the upper mantle can be milder than that on surface waves (Yoshizawa et al, 1999), in addition to the relatively smaller influence from anisotropy on P-waves compared to surface waves (Crampin et al, 1982).

Recently, major seismological data centers, such as EarthScope (formerly IRIS: Incorporated Research Institutions for Seismology), have provided us with more precise information on the station orientation for their affiliated stations worldwide, including Australian stations. Given proper information from careful calibrations, many of the broadband horizontal channels in major stations in global networks (such as the Global Seismograph Network) have been named BH1 and BH2 (for the first and second components) rather than conventional BHN and BHE (North and East), when the true horizontal directions deviate from the geographic north and east (Ekström and Busby, 2008). Ekström (2008) has also provided practically useful tables on the station orientation for GSN stations until 2015. However, a number of seismic stations from local data providers and temporary seismic networks, including transportable seismic arrays (e.g., SKIPPY in Australia; Hilst et al, 1994), still lack precise information on horizontal orientations, which is crucial for researchers wishing to utilize these valuable waveform data sets.

In this paper, we collect a large number of P-wave arrival angle data to estimate the horizontal orientation of many broadband seismic stations in Australia, modeled on the method of polarization analysis by Vidale (1986) utilized in earlier study by Yoshizawa et al (1999). Through the polarization analysis of teleseismic P-wave particle motions, we construct a complete catalog of the horizontal orientation of currently available broadband stations in Australia, which can be used for a variety of future applications of seismic data analyses with horizontal components.

2 Data and Method

2.1 Data

We used the three-component teleseismic P-wave data downloaded from the EarthScope Data Management Center (EarthScope DMC) and Australian Passive Seismic Server (AusPass) for 4004 seismic events with moment magnitude Mw $\geq$ 5.5 from 1987 to 2019. Our dataset includes both permanent and temporary broadband stations shown in Figures 1 (a, b). Permanent seismic networks include IRIS/IDA (red triangles in Figure 1 (a); Network II, Scripps Institution of Oceanography (1986)), IRIS/USGS (purple triangles in Figure 1 (a); Network IU, Albuquerque Seismological Laboratory/USGS (1988)), GEOSCOPE (green triangles in Figure 1 (a); Network G, Institut de physique du globe de Paris (IPGP) and École et Observatoire des Sciences de la Terre de Strasbourg (EOST) (1982)), GeoScience Australia (blue triangles in Figure 1 (a); Network AU, Geoscience Australia (2021)), and Australian Seismometers in Schools program (orange triangles in Figure 1 (a); Network S1, Salmon et al (2011)). Temporary stations shown in Figure 1 (b) involve many temporary seismic arrays, SKIPPY (7B) (Hilst and Kennett, 1993), KIMBA (7D and 7E) (Kennett, 1997, 1998), QUOLL (7F) (Kennett et al, 1999), West Australia Cratons (7G) Kennet (2000), TRIGGER BB (7H) (Rawlinson and Kennett, 2001), TASMAL (7I) (Kennett, 2003), CARPA - Linkage (7J) (Reading and Kennett, 2005), SOC - Southern Craton (7K) (Fontaine and Kennet, 2007), BILBY (6F) (Rawlinson and Kennet, 2008), Bass Strait (1P) (Reading and Rawlinson, 2011), Southern Queensland Spiral Array (SQSPA; 1E) (Tkalčić et al, 2013b), Albany-Fraser Experiment (1K) (Tkalčić et al,

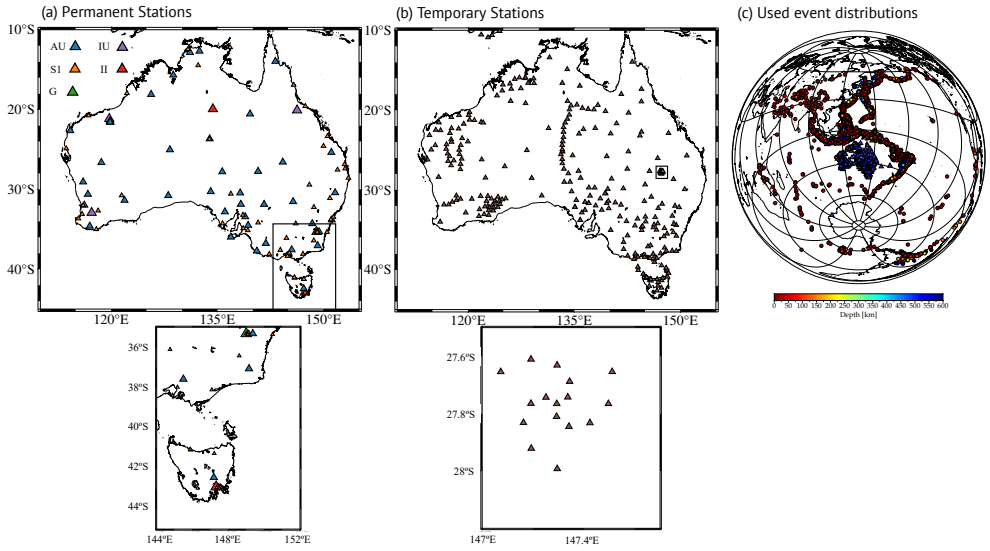

Fig. 1 Broadband seismic stations and seismic events used in this study. (a) Permanent stations, with colors indicating different networks (AU, S1, IU, II, and G). (b) Temporary stations. (c) Seismic events used in this study, with colors representing source depths. Blue triangles are employed stations in (a) and (b). For (a) and (b), magnified figures for the encompassed areas by rectangles are displayed below each panel.

2013a), and Transitions in the Banda Arc-Australia continental collision (1G) (Miller, 2014).

2.2 Method of P-wave polarization analysis

We employed the complex time-domain polarization analysis of Vidale (1986) to measure P-wave arrival angles from three-component direct P-wave seismograms. This method has been widely used for the polarization analysis of various seismic phases, including an earlier study on misorientation corrections (e.g., Yoshizawa et al, 1999).

First, we converted the time-series waveforms into analytic signals to construct the covariance matrix of the three-component seismograms, with the covariance averaged over 1 second. We then computed the eigenvalues and corresponding eigenvectors of the covariance matrix and solved the minimization problem associated with the inverse of equation (4) in Vidale (1986). This procedure was applied from 80 s before to 60 s after the P-wave arrival, and yielded estimates of the arrival angle, ellipticity (or linearity), and incident angle of the direct P-waves. Details of practical data processing based on this polarization analysis are summarized in the next subsection.

2.3 Data processing

We selected seismic events with Mw $\geq$ 5.5, distance ranges between 30 and 90 degrees, and normalized amplitude of P-wave radiation $>$ $|0.3|$ estimated from the Global CMT catalog (Dziewonski et al, 1981; Ekström et al, 2012). We first corrected the

instrument response, converted the waveform data into the displacement, and applied a bandpass filter between 0.03 and 0.1 Hz. Second, we rotated the two horizontal waveforms into the radial and transverse components based on the station catalog information of horizontal orientation provided by EarthScope DMC and AusPass. To discard the low-quality data, we calculated signal-to-noise ratios (SNR) in the vertical and radial components and removed data with vertical SNR < 5.0 and radial SNR $<$ 3.0. Then, for each seismic event and station, we performed a time-domain complex polarization analysis of Vidale (1986) to measure the horizontal arrival angles Θ of direct P-waves in a similar way to Yoshizawa et al (1999), which is summarized in Figure 2. Since teleseismic P-wave typically exhibit linear particle motion in the radial-vertical plane, we applied a data selection criterion requiring the ellipticity parameter P_E to be smaller than 0.175, which was determined empirically. Third, we calculated the median of the time-dependent arrival angles for each event (an orange line in the third panel in Figure 2 (a)) in a selected time window. In this study, we set the time window as 7.5 s before and after the main P-wave pulse (Figure 2 (a)). Consequently, in the final step, we compiled a large number of arrival angle data from many seismic events to evaluate the misorientation of horizontal sensors.

Finally, in this study, we adopted the median as a representative measure of arrival-angle anomalies (i.e., deviations from the great-circle direction) over the selected observation period (Figure 2 (b)). The distribution of earthquakes around Australia for teleseismic P-wave analysis is concentrated primarily in the north and east (Figure 1 (c)). This back-azimuthal bias can unintentionally affect the sensor orientation estimates when using the arithmetic mean, as events from dominant directions may bias the result. To mitigate this issue, we adopted the median, which is less sensitive to uneven azimuthal distributions and provides a more robust estimate of central tendency. Nevertheless, we also included the mean values in our catalog (Tables S1–S3 and Tarumi and Yoshizawa (2024)) for comparison. This final step was applied to stations with more than 5 arrival-angle measurements, and several stations with large uncertainties in the time-dependent polarization data were excluded based on visual inspection. The resulting distribution of all events used in this study is shown in Figure 1 (c).

Station metadata (or catalog information of horizontal orientation provided by EarthScope) for permanent stations is subject to change from time to time, reflecting irregular maintenance, calibrations, and replacement of instruments. For the permanent stations with a long observation period, we visually inspected the timing of sudden changes in the trend of estimated horizontal misorientation, allowing us to detect some temporal changes at unreported (i.e., not included in the EarthScope catalog) timings (e.g., AU.COEN in Figure 3 (f)). For the estimation of horizontal misorientation, we divide the period windows in which the median of measured arrival angles is computed, depending on each station, as shown in Figures 2 (b) and 3.

3 Results

Our arrival-angle measurements enabled us to detect probable misorientations from the geographic north for permanent and temporary stations (Figures 2, 3, 4, 5, and

S7). All results are summarized in Supplementary Materials 2 (Tables S1–S3) and Zenodo Repositiory (Tarumi and Yoshizawa, 2024). In this section, we explain our results on the permanent and temporary stations separately.

3.1 Permanent Stations

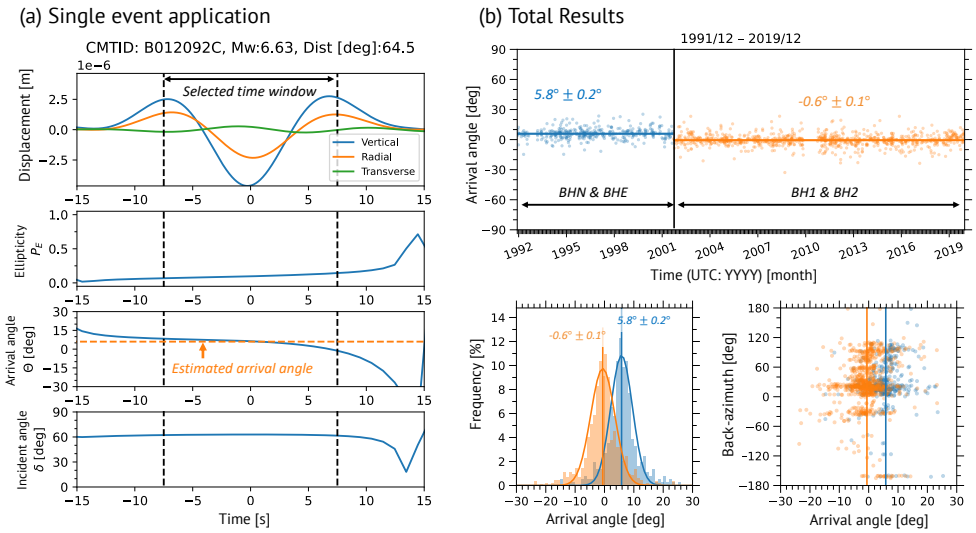

Fig. 2 A visual summary of P-wave polarization analysis for IU.NWAO. (a) An example of teleseismic P-wave for an event at the epicentral distance of 64.5 degrees and the estimated polarization parameters. From top to bottom: three-component displacement waveforms rotated to the catalog values of EarthScope metadata (blue: vertical; orange: radial; green: transverse), ellipticity P_E, arrival angle Θ on a horizontal plane, and incident angle δ for the P-wave particle motion. The arrival angle is measured clockwise from the radial (great-circle) direction so that a positive deviation indicates the arrival-angle anomaly to the east. In the third panel, a dashed orange line exhibits a median value in the selected time window encompassed by vertical dashed lines. (b) Compiled P-wave polarization data for all events used for the NWAO station. The top panel represents the time series of P-wave arrival angles. The colors for dots and lines represent the distinct period characterized by different trends of arrival angles. The timing of the arrival-angle trend change in September 2001 (indicated by a solid vertical line) matched well with the reported (i.e., included in the EarthScope catalog) correction of horizontal components by EarthScope. The bottom-left panel shows histograms and fitted Gaussian functions for each period, and the bottom-right one indicates the back-azimuth dependence of the measured arrival angles for all employed events. In the top and bottom-left panels, the estimated station orientations and standard errors are labeled. The colors of the characters correspond to each distinct time period.

Figure 2 shows the summary of P-wave polarization measurements for IU.NWAO which has been a long-running station located in southeast Australia since 1992. According to the EarthScope metadata catalog, the channel name of the horizontal components was changed from BHN/BHE to BH1/BH2 in September 2001. Our measured P-wave arrival angles show apparent temporal changes in the polarization trend

at this time. The misorientation angle of horizontal sensors was estimated to be about 5.8° before September 2001, and it has decreased to 0.6° since then (by 2019, at least), indicating the improvement in the catalog information of this station.

Note that, for this station, Laske and Masters (1996), Yoshizawa et al (1999), and Schulte-Pelkum et al (2001), who employed the particle motion of either Rayleigh wave or teleseismic P-wave before 2000, have already estimated the misalignment from the north by around 5°. In particular, our estimated misorientation angle (5.8°) before September 2001 in Figure 2 (b) is very close to the estimated value by Schulte-Pelkum et al (2001), who employed the P wave data in the same period. Fontaine et al (2009) also used similar P-wave datasets and identified a misalignment of 5°, which is consistent with our results. For the other GSN stations used in this study, our estimated orientations are generally in agreement with the earlier online report (Ekström, 2008).

In addition to temporal changes, we can also see a back-azimuthal dependence in the arrival-angle data (Figure 2 (b, bottom-right panel)). Such azimuthal variations of arrival angles can also be observed at other stations, which may be worth further investigation in the future, since they may reflect lateral variations in heterogeneity and azimuthal anisotropy, including dipping interfaces, in the upper mantle beneath the seismic station (Schulte-Pelkum et al, 2001; Fontaine et al, 2009). Additionally, when the event distribution does not cover the full azimuthal range, such a back-azimuthal dependence can unintentionally bias the arithmetic mean of arrival angles. Therefore, our choice of the median should effectively suppress such unfavorable weighting.

Figure 3 shows a summary of P-wave polarization data (arrival-angle anomalies from the great-circle path for each event) for six permanent and two temporary stations during their operation periods until 2019. The horizontal-component channels of these stations have been labeled as BHN/BHE since their installation. At G.CAN (Canberra by GEOSCOPE; Figure 3 (a)), the station orientation estimated in this study is nearly 0° (Tables S1–S3 in Supplementary Materials), suggesting that this seismometer has been accurately aligned with the geographic north and east. AU.TOO (Figure 3 (b)) also shows no significant temporal changes, though our measurements suggest a slight misalignment (about -1.2°) from the north, which can be almost negligible. At AU.BBOO and AU.KMBL stations (Figure 3 (c, d)), we can see clear temporal changes in the trends of polarization angles, which coincide well with the timing of reported maintenance and/or instrument replacement. On the other hand, at AU.STKA and AU.COEN (Figure 3 (e, f)), unknown temporal changes in polarization angles are detected at unreported timings. In particular, STKA exhibits a very large misalignment of about 30° from north since the early stage of its operation.

Compiled maps of the estimated horizontal misorientations for permanent stations are displayed in Figure 4, in which we show the misorientations in each period in Figures 4 (a-e), and those compiled for the entire period of our analysis in Figure 4 (f). For permanent stations, including those in the S1 network, the station misorientations and their standard errors are summarized in time-dependent horizontal bar graphs in Figures S1, S2, and S5 in Supplementary Material 1 (hereafter SM1) and are separately tabulated in Tables S1 and S2 in Supplementary Material 2 (hereafter

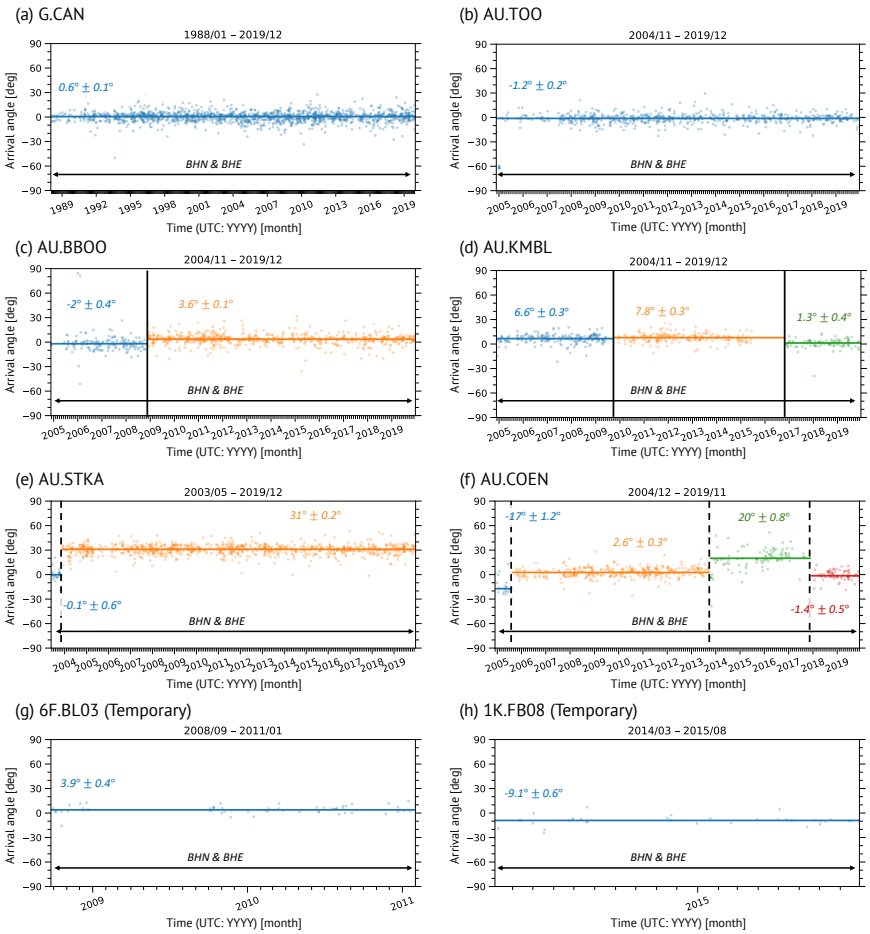

Fig. 3 Time-dependent P-wave polarization data (arrival-angle deviation from the great circle) for selected stations, (a-f) permanent stations installed and maintained by GEOSCOPE (G) and Geoscience Australia (AU), and (g, h) temporary stations. Notations in these figures are the same as 2 (b, top panel). The vertical black lines represent the timing of significant trend changes in P-wave arrival angles. Solid vertical lines indicate the timing of the reported maintenance and/or replacement of instruments, and dashed vertical lines represent unknown temporal changes at unreported timings (i.e., not documented in the EarthScope catalog). As described in the main text, no temporal changes were identified for temporary stations.

SM2). In particular, we can identify significant time-dependent variations of misorientations for AU stations. These temporal changes mostly coincide with the reported timing of maintenance and/or replacement by the EarthScope and AusPass. However, such temporal changes at several stations (e.g., AU.COEN) are found at unreported timings. The misorientation of some permanent stations from the geographic north is more than 10°, which may affect seismic waveform analysis, especially when using the horizontal components. Figure S6 (SM1) demonstrates the three-component seismograms observed at STKA to compare waveforms before and after correcting the station

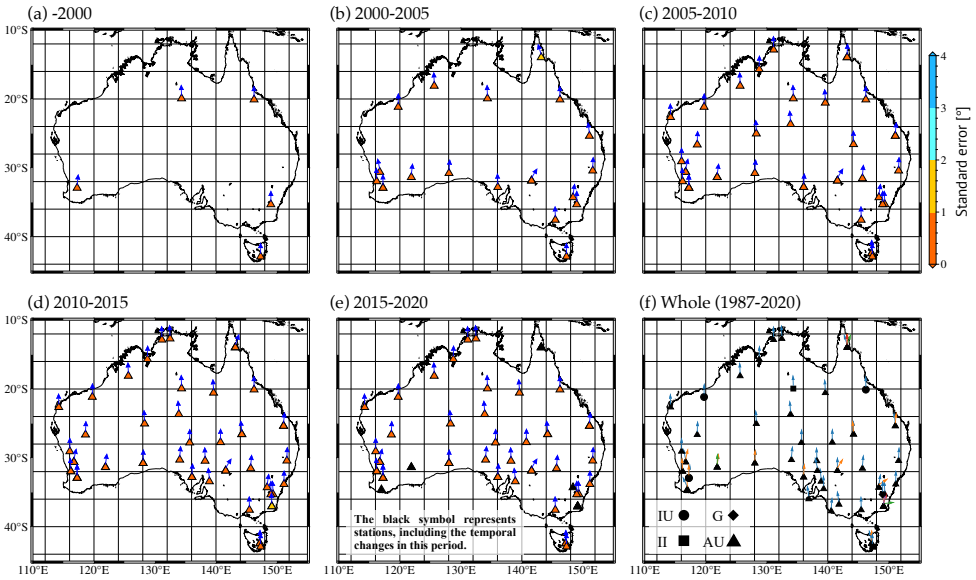

Fig. 4 Map projections of horizontal misorientations from the geographic north for permanent seismic stations (II, IU, G, and AU) in Australia. (a-e) Arrows indicate the median directions of horizontal sensors over the designated period. Colors in the triangles indicate the estimated standard errors shown in the color bar on the right. Black triangles without arrows indicate stations with varying misorientations during the period. (f) A compiled map of estimated misorientations for the whole period of analysis. The colors of arrows indicate the horizontal sensor orientations in different periods. Black symbols indicate stations of different seismic networks.

misorientations. In Figure S6 (a) in SM1, we can see the apparent energy leakage of the P-wave from the radial to transverse component. In Section 4, we will discuss the effects of the station correction on azimuth-dependent receiver function analyses.

Some stations in AU exhibit relatively large standard errors compared to others (e.g., AU.ARPS; AU.MANU; see Figure S1 and Table S1). These larger uncertainties may be influenced by the limited number of data samples and/or the back-azimuthal dependence of arrival angles.

For AU stations, we compare our measurements with those from a recent study in Table 1; we present our estimated misalignments for selected AU stations, along with PKS/SKS-based measurements from Eakin et al (2023). We focused on stations for which Eakin et al (2023) estimated non-zero misalignments, comparing them with the most recent misorientation data from our catalog between 1987 and 2019. Our measurements are generally in good agreement with those of Eakin et al (2023). Note that large misalignment at AU.STKA is identical between both studies.

For another permanent network, S1 (Salmon et al, 2011), we obtained reliable misorientation estimates for only 13 stations. Although the use of the S1 network is outside the primary scope of our study, which focuses on the waveform analysis of high-quality broadband seismic records, we include the results for the S1 network in Figures S5 and S8, Table S2, and Section S1.

Table 1 Comparison of recent misalignment measurements at AU stations by Eakin et al (2023) and this study. Eakin et al (2023) estimated these using PKS and/or SKS phases, as indicated. In the third column showing our results, the data period and the number of seismic events used are shown (e.g., 2011–2019; 100).

Station	Eakin et al (2023) (PKS and/or SKS)	This study (Teleseismic P-wave)
AU.ARPS	-6° (SKS)	-9.4°±4.4° (2019; 6)
AU.FORT	0° (PKS), 3.5° (SKS)	4.4°±0.4° (2003–2011; 69) 1.4°±0.2° (2011–2019; 404)
AU.HTT	-4° (PKS), -3° (SKS)	-6.3°±0.2° (2010-2019; 399)
AU.KELC	-6° (SKS)	-9°±1.3° (2019; 19)
AU.MGBR	-10° (SKS)	4.4°±1.8° (2019; 30)
AU.MILA	6° (SKS)	1.7°±0.6° (2011–2014; 44) -2.5°±1.6° (2014–2016; 22) 83°±0.9° (2016–2018; 18) 17°±1.1° (2018–2019; 17) 6.5°±1.0° (2019; 12)
AU.MULG	6.6° (PKS & SKS)	5.0°±0.4° (2013–2019; 219)
AU.SDAN	2.5° (SKS)	-1.5°±0.7° (2018–2019; 48)
AU.STKA	31° (PKS & SKS)	-0.1°±0.6° (2003; 23) 31.0°±0.2° (2003–2019; 899)
AU.YAPP	-13.4° (PKS & SKS)	-13°±0.5° (2018–2019; 55)
AU.YNG	5° (PKS), 10° (SKS)	8.7°±0.3° (2004–2017; 429) 56°±1.2° (2017–2019; 42)

3.2 Temporary Stations

The seismic records of temporary stations are generally less than two years long, and we could not find any significant temporal changes in the horizontal orientation. Figures 3 (g) and (h) show examples of a time-dependent polarization measurement for selected temporary stations. As expected from the limited data acquisition period, we could not observe any significant temporal changes in the time-series data of these stations. In Figure 5, we compiled the station orientation for all temporary stations that met the criteria described in Section 2. Also, we summarized the station orientations and their standard errors in Figures S3 and S4 and Table S3 in Supplemental Materials. While some stations exhibit relatively large misalignments, the horizontal sensors at almost all temporary stations generally align with the geographic north and east directions (Figures 5 and S3), suggesting proper installation. We also compare PKS/SKS-based measurements from Eakin et al (2023) and teleseismic P-wave measurements from this study in Table 2, similar to the previous subsection. Overall, for most temporary stations, our results are generally consistent with those of Eakin et al (2023). The discrepancies at some stations may be attributed to the utilized recording periods, the measurement quality for different seismic phases, and the number of employed events.

4 Discussion and Conclusions

In this section, we briefly examine the effect of the station correction on P-wave receiver function (P-RF) analysis. We computed the P-RFs at AU.STKA, where a large misorientation of over 30° was observed, and analyzed the differences between

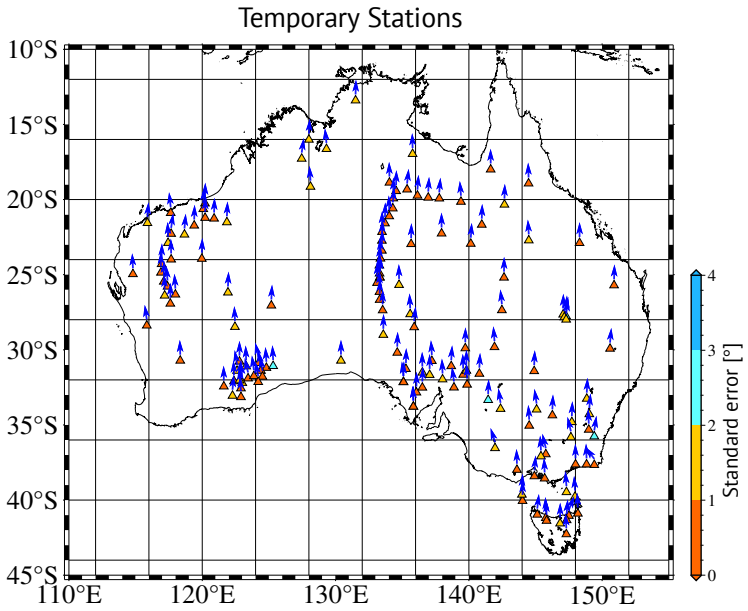

Fig. 5 Station misorientations from the geographic north in a horizontal sensor for temporary seismic stations.

Table 2 Same as Table 1, but for selected temporary stations.

Station	Eakin et al (2023) (PKS and/or SKS)	This study (Teleseismic P-wave)
1E.SQA01	5° (SKS)	3.0°±2.4° (2013–2014; 7)
1E.SQA09	10° (SKS)	16.0°±1.4° (2013–2014; 7)
1E.SQA11	10° (SKS)	9.2°±1.3° (2013–2014; 7)
1P.BA12	-25° (SKS)	-36.0°±0.9° (2011-2013; 9)
1P.BA13	0° (SKS)	-1.8°±0.8° (2011–2013; 26)
1P.BA19	9° (SKS)	-2.7°±0.8° (2011–2013; 16)
7H.TB03	5° (SKS)	-3.0°±1.0° (2011-2013)
7I.GA06	-5° (PKS), 0° (SKS)	-6.3°±0.9° (2004; 7)
7I.GA08	-5° (SKS)	-3.4°±0.9° (2004–2005; 10)
7I.TL10	-7° (PKS & SKS)	-6.1°±0.8° (2003–2005; 19)
7I.TL14	0° (PKS), 8° (SKS)	-4.4°±0.7° (2003–2005; 38)
7I.TL17	5° (SKS)	-1.4°±0.4° (2003–2005; 30)
7K.SOC03	0° (PKS), 5° (SKS)	2.7°±1.26° (2007–2008; 6)

uncorrected and corrected P-RF data for both radial and transverse components. In these calculations, we considered the azimuthal dependence of P-RFs, which arises from the varying incoming directions (or back-azimuths) of teleseismic P-wave. The azimuth-dependent radial P-RFs reflect lateral variations in seismic discontinuities around the station (e.g., Tonegawa et al, 2005; Kawakatsu et al, 2009; Kumar and Kawakatsu, 2011). In addition, incorporating transverse P-RFs enables us to infer seismic anisotropy in the crust and upper mantle (e.g., Park and Levin, 2016; Shiomi, 2017; Birkey and Ford, 2023). Significant uncertainties in the horizontal component orientations could lead to misinterpretations in the results of P-RF analysis.

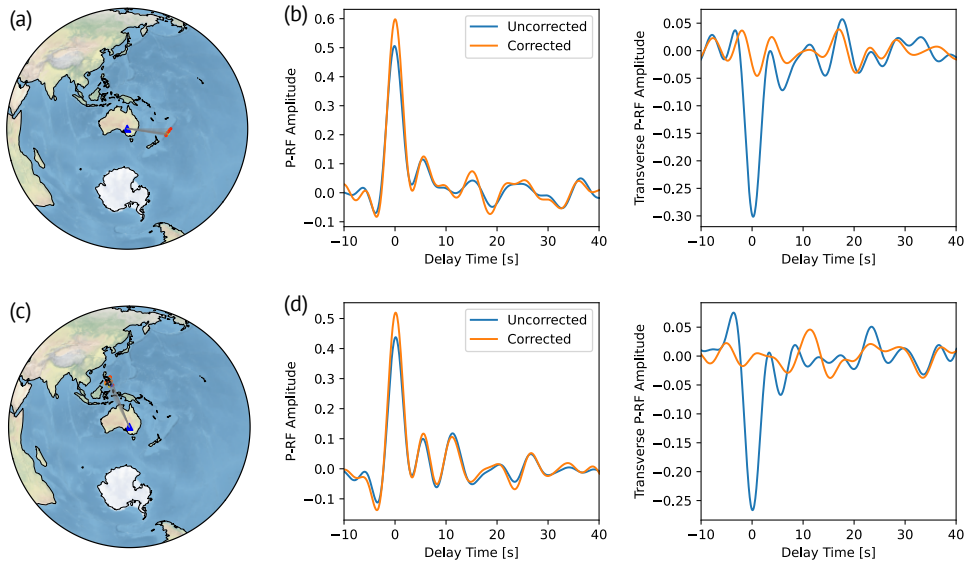

Fig. 6 Comparison of P-wave receiver functions (P-RFs) for AU.STKA. (a, c) Maps showing event groups used for the P-RF analysis. (b) Stacked radial and transverse P-RFs for the eastern events shown in (a). Blue and orange lines represent P-RFs from uncorrected and corrected teleseismic P-wave data, respectively. (d) Same as (b), but for the northwestern events shown in (c).

Figure S6 in Supplementary Material 1 shows an example of teleseismic P-wave records observed at AU.STKA before and after the correction for station orientation, clearly indicating the energy leakage of P-wave from radial to transverse in the uncorrected horizontal traces. Using these two sets of teleseismic P-wave data, we computed radial and transverse P-RFs for two incoming directions within narrow distance ranges (10°) (Figure 6 (a, c)). After calculating individual P-RFs, we selected P-RF traces using the cross-correlation coefficient (CC)-based selection method (Tkalčić et al, 2011), stacking all traces with CC > 0.7. The resulting stacked P-RF traces are shown in Figure 6 (b, d), and the stacking process is visually summarized in Figures S8 and S9 in Supplementary Material 1. The radial P-RFs are generally consistent regardless of the correction of misorientation. Still, the relative amplitude of converted phases for the direct P-wave can be modulated, potentially affecting analyses that rely on RF amplitude. For the transverse RFs, clear differences emerge between the uncorrected and corrected P-RF traces. In the uncorrected transverse P-RFs, we can see clear signals of direct P-wave, Moho-converted phases, and their multiple reflections, contaminating the P-to-SH converted phases. This contamination prevents us from properly interpreting P-to-SH conversions, which can be generated by anisotropic properties or oblique interfaces. Therefore, proper corrections of station azimuths during the waveform processing are essential for the accurate interpretation of both radial and transverse P-RF amplitudes.

In this study, we constructed a comprehensive station orientation catalog for Australian broadband seismic stations by analyzing long-period teleseismic P-wave particle

motion data. The catalog includes temporal variations in station misorientations. While the timing of these changes is generally consistent with that reported in the EarthScope catalog, some stations exhibit changes at unexpected times. Finally, we assessed the utility of our catalog for receiver function analysis, demonstrating that correcting for station misorientation can significantly affect the amplitude analysis of RFs, particularly in the transverse component.

Acknowledgment

We thank Sima Mousavi and an anonymous reviewer for their thorough reviews, constructive suggestions, and insightful comments, which were very helpful in improving the original manuscript. All seismograms used in this study were obtained from the EarthScope Data Management Center (https://ds.iris.edu/ds/nodes/dmc/) and the Australian Passive Seismic Server (AusPass; https://auspass.edu.au/index.html). We used ObsPy (Beyreuther et al, 2010) for downloading and analyzing all seismic waveform data. We used matplotlib (Hunter, 2007), cartopy (Met Office, 2010), Generic Mapping Tools (Wessel et al, 2019), and PyGMT (Uieda et al, 2021) to create all figures.

Data Availability

The numerical data for our station misorientation catalog are included in PDF files provided as part of Supplementary Materials and Zenodo Repository (Tarumi and Yoshizawa, 2024). A sample Python script for the polarization analysis used in this study is also available from the same Zenodo repository. All teleseismic waveform data used in this study are available from the EarthScope Data Management Center (https://ds.iris.edu/ds/nodes/dmc/) and the Australian Passive Seismic Server (AusPass; https://auspass.edu.au/index.html). The networks used in this study are: II (Scripps Institution of Oceanography, 1986); IU (Albuquerque Seismological Laboratory/USGS, 1988); G (Institut de physique du globe de Paris (IPGP) and École et Observatoire des Sciences de la Terre de Strasbourg (EOST), 1982); AU (Geoscience Australia, 2021); S1 (Salmon et al, 2011); 7B (Hilst and Kennett, 1993); 7D (Kennett, 1997); 7E(Kennett, 1998); 7F (Kennett et al, 1999); 7G (Kennet, 2000); 7H (Rawlinson and Kennett, 2001); 7I (Kennett, 2003); 7J (Reading and Kennett, 2005); 7K (Fontaine and Kennet, 2007); 6F (Rawlinson and Kennet, 2008); 1P (Reading and Rawlinson, 2011); 1E (Tkalčić et al, 2013b); 1K (Tkalčić et al, 2013a); 1G (Miller, 2014).

Funding

This study was partly supported by JST SPRING grant number JPMJSP2119 to KT and JSPS KAKENHI (grant number 24KJ0294 to KT; 20K04096 and 23K03539 to KY).

Competing Interests

The authors have no relevant financial or non-financial interests to disclose.

Author Contributions

KT: Conceptualization, Data curation, Methodology, Formal analysis, Funding acquisition, Investigation, Visualization, Software, Writing - Original draft; KY: Conceptualization, Data curation, Methodology, Funding acquisition, Investigation, Supervision, Project Administration, Writing – review and editing

References

Albuquerque DF, Rocha MP, Ianniruberto M, et al (2024) Estimating seismometer component orientation of the Brazilian seismographic network using teleseismic P-wave particle motion analysis and directional statistics. Journal of South American Earth Sciences 134:104754. https://doi.org/10.1016/j.jsames.2023.104754

Albuquerque Seismological Laboratory/USGS (1988) Global seismograph network (gsn - iris/usgs). https://doi.org/10.7914/SN/IU, URL https://www.fdsn.org/networks/detail/IU/

Beyreuther M, Barsch R, Krischer L, et al (2010) ObsPy: A Python Toolbox for Seismology. Seismological Research Letters 81(3):530–533. https://doi.org/10.1785/gssrl.81.3.530

Birkey A, Ford HA (2023) Anisotropic structure of the Australian continent. Frontiers in Earth Science 10:1055480. https://doi.org/10.3389/feart.2022.1055480

Crampin S (1975) Distinctive Particle Motion of Surface Waves as a Diagnostic of Anisotropic Layering. Geophysical Journal of the Royal Astronomical Society 40(2):177 – 186. https://doi.org/10.1111/j.1365-246x.1975.tb07045.x, URL http://dx.doi.org/10.1111/j.1365-246X.1975.tb07045.x

Crampin S, Stephen RA, McGonigle R (1982) The polarization of P-waves in anisotropic media. Geophysical Journal of the Royal Astronomical Society 68(2):477–485. https://doi.org/10.1111/j.1365-246x.1982.tb04910.x, URL http://dx.doi.org/10.1111/j.1365-246X.1982.tb04910.x

Deng W, Han G, Li J, et al (2024) Seismometer orientation measurements of broadband seismic stations in the china digital seismograph network. Bulletin of the Seismological Society of America https://doi.org/10.1785/0120240075

Dziewonski AM, Chou T, Woodhouse JH (1981) Determination of earthquake source parameters from waveform data for studies of global and regional seismicity. Journal of Geophysical Research: Solid Earth 86(B4):2825–2852. https://doi.org/10.1029/jb086ib04p02825

Eakin CM, Davies DR, Ghelichkhan S, et al (2023) The Influence of Lithospheric Thickness Variations Beneath Australia on Seismic Anisotropy and Mantle Flow. Geochemistry, Geophysics, Geosystems 24(9). https://doi.org/10.1029/2023gc011066

Ekström G (2008) Polarization anomalies at various stations. URL https://www.ldeo.columbia.edu/~ekstrom/Projects/WQC/COMB_QC/

Ekström G, Busby RW (2008) Measurements of Seismometer Orientation at USArray Transportable Array and Backbone Stations. Seismological Research Letters 79(4):554–561. https://doi.org/10.1785/gssrl.79.4.554

Ekström G, Dalton CA, Nettles M (2006) Observations of Time-dependent Errors in Long-period Instrument Gain at Global Seismic Stations. Seismological Research Letters 77(1):12–22. https://doi.org/10.1785/gssrl.77.1.12

Ekström G, Nettles M, Dziewoński A (2012) The global CMT project 2004–2010: Centroid-moment tensors for 13,017 earthquakes. Physics of the Earth and Planetary Interiors 200:1–9. https://doi.org/10.1016/j.pepi.2012.04.002

Fontaine F, Kennet B (2007) SOC - Southern Craton. URL https://www.fdsn.org/networks/detail/7K_2007/

Fontaine FR, Barruol G, Kennett BLN, et al (2009) Upper mantle anisotropy beneath Australia and Tahiti from P wave polarization: Implications for real-time earthquake location. Journal of Geophysical Research: Solid Earth 114(B3). https://doi.org/10.1029/2008jb005709

Geoscience Australia (2021) Australian national seismograph network data collection. https://doi.org/10.26186/144675, URL http://pid.geoscience.gov.au/dataset/ga/144675

Hejrani B, Tkalčić H (2020) Resolvability of the Centroid-Moment-Tensors for Shallow Seismic Sources and Improvements From Modeling High-Frequency Waveforms. Journal of Geophysical Research: Solid Earth 125(7). https://doi.org/10.1029/2020jb019643

Hilst Rvd, Kennett B (1993) SKIPPY. URL https://www.fdsn.org/networks/detail/7B_1993/

Hilst Rvd, Kennett B, Christie D, et al (1994) Project Skippy explores lithosphere and mantle beneath Australia. Eos, Transactions American Geophysical Union 75(15):177–181. https://doi.org/10.1029/94eo00857

Hunter JD (2007) Matplotlib: A 2D Graphics Environment. Computing in Science & Engineering 9(3):90–95. https://doi.org/10.1109/mcse.2007.55

Institut de physique du globe de Paris (IPGP), École et Observatoire des Sciences de la Terre de Strasbourg (EOST) (1982) Geoscope, french global network of broad band seismic stations. https://doi.org/10.18715/GEOSCOPE.G, URL http://geoscope.ipgp.fr/networks/detail/G/

Kawakatsu H, Kumar P, Takei Y, et al (2009) Seismic Evidence for Sharp Lithosphere-Asthenosphere Boundaries of Oceanic Plates. Science 324(5926):499–502. https://doi.org/10.1126/science.1169499

Kennet B (2000) West Australian Cratons. URL https://www.fdsn.org/networks/detail/7G_2000/

Kennett B (1997) KIMBA97. URL https://www.fdsn.org/networks/detail/7D_1997/

Kennett B (1998) KIMBA98. URL https://www.fdsn.org/networks/detail/7E_1998/

Kennett B (2003) TASMAL. URL https://www.fdsn.org/networks/detail/7I_2003/

Kennett B, Debayle E, Gorbatov A (1999) QUOLL. URL https://www.fdsn.org/networks/detail/7F_1999/

Kennett BLN, Furumura T (2008) Stochastic waveguide in the lithosphere: Indonesian subduction zone to Australian craton. Geophysical Journal International 172(1):363 – 382. https://doi.org/10.1111/j.1365-246x.2007.03647.x, URL http://doi.wiley.com/10.1111/j.1365-246X.2007.03647.x

Kennett BLN, Fichtner A, Fishwick S, et al (2013) Australian Seismological Reference Model (AuSREM): mantle component. Geophysical Journal International 192(2):871–887. https://doi.org/10.1093/gji/ggs065, URL http://gji.oxfordjournals.org/content/192/2/871.full

Kumar P, Kawakatsu H (2011) Imaging the seismic lithosphere-asthenosphere boundary of the oceanic plate. Geochemistry, Geophysics, Geosystems 12(1):n/a–n/a. https://doi.org/10.1029/2010gc003358

Larson EWF, Ekström G (2002) Determining surface wave arrival angle anomalies. Journal of Geophysical Research 107(B6). https://doi.org/10.1029/2000jb000048

Laske G (1995) Global observation of off-great-circle propagation of Long-Period surface waves. Geophysical Journal International 123(1):245 – 259. https://doi.org/10.1111/j.1365-246x.1995.tb06673.x, URL http://gji.oxfordjournals.org/content/123/1/245.abstract

Laske G, Masters G (1996) Constraints on global phase velocity maps from long-period polarization data. Journal of Geophysical Research: Solid Earth 101(B7):16059–16075. https://doi.org/10.1029/96jb00526

Met Office (2010) Cartopy: a cartographic python library with a Matplotlib interface. URL https://scitools.org.uk/cartopy

Miller MS (2014) Transitions in the Banda Arc-Australia continental collision. URL https://www.fdsn.org/networks/detail/1G_2019/

Park J, Levin V (2016) Anisotropic shear zones revealed by backazimuthal harmonics of teleseismic receiver functions. Geophysical Journal International 207(2):1216–1243. https://doi.org/10.1093/gji/ggw323

Rawlinson N, Kennett B (2001) TIGGER BB. URL https://www.fdsn.org/networks/detail/7H_2001/

Rawlinson S, Kennet B (2008) BILBY. URL https://www.fdsn.org/networks/detail/6F_2008/

Reading A, Kennett B (2005) CAPRA - Linkage. URL https://www.fdsn.org/networks/detail/7J_2005/

Reading A, Rawlinson N (2011) Bass Strait. URL https://www.fdsn.org/networks/detail/1P_2011/

Salmon M, Balfour N, Sambridge M (2011) Australian Seismometers in Schools. URL https://www.fdsn.org/networks/detail/S1/

Schulte-Pelkum V, Masters G, Shearer PM (2001) Upper mantle anisotropy from long-period P polarization. Journal of Geophysical Research: Solid Earth 106(B10):21917–21934. https://doi.org/10.1029/2001jb000346

Scripps Institution of Oceanography (1986) Global seismograph network - iris/ida. https://doi.org/10.7914/SN/II, URL https://www.fdsn.org/networks/detail/II/

Shiomi K (2017) Dissimilar receiver functions observed at very close stations in the Kii Peninsula, central Japan: features and causes. Earth, Planets and Space 69(1):48. https://doi.org/10.1186/s40623-017-0631-5

Sun W, Tkalčić H, Tang Q (2024) Single-Station Back-Azimuth Determination with the Receiver Function Rotation Technique Validated by the Locations of Earthquakes, Impacts, and Explosions. Seismological Research Letters https://doi.org/10.1785/0220240117

Tarumi K, Yoshizawa K (2024) Numerical Sheet for "Station-orientation catalog for Australian broadband seismic stations". URL https://doi.org/10.5281/zenodo.16901548

Tkalčić H, Chen Y, Liu R, et al (2011) Multistep modelling of teleseismic receiver functions combined with constraints from seismic tomography: crustal structure beneath southeast China. Geophysical Journal International 187(1):303–326. https:

//doi.org/10.1111/j.1365-246x.2011.05132.x

Tkalčić H, Kennett B, Sippl C, et al (2013a) Albany-Fraser Experiment. URL https://www.fdsn.org/networks/detail/1K_2013/

Tkalčić H, Kennett B, Tanaka S, et al (2013b) Southern Queensland Spiral Array. URL https://www.fdsn.org/networks/detail/1E_2013/

Tonegawa T, Hirahara K, Shibutani T (2005) Detailed structure of the upper mantle discontinuities around the Japan subduction zone imaged by receiver function analyses. Earth, Planets and Space 57(1):5–14. https://doi.org/10.1186/bf03351801

Uieda L, Tian D, Leong WJ, et al (2021) PyGMT: A Python interface for the Generic Mapping Tools https://doi.org/10.5281/zenodo.5607255, URL https://doi.org/10.5281/zenodo.5607255, the development of PyGMT has been supported by NSF grants OCE-1558403 and EAR-1948603.

Vidale JE (1986) Complex polarization analysis of particle motion. Bulletin of the Seismological Society of America 76(5):1393–1405. https://doi.org/10.1785/bssa0760051393, URL https://doi.org/10.1785/BSSA0760051393

Wessel P, Luis JF, Uieda L, et al (2019) The Generic Mapping Tools Version 6. Geochemistry, Geophysics, Geosystems 20(11):5556–5564. https://doi.org/10.1029/2019gc008515

Yoshizawa K (2014) Radially anisotropic 3-D shear wave structure of the Australian lithosphere and asthenosphere from multi-mode surface waves. Physics of the Earth and Planetary Interiors 235:33–48. https://doi.org/10.1016/j.pepi.2014.07.008, URL http://www.sciencedirect.com/science/article/pii/S0031920114001745

Yoshizawa K, Yomogida K, Tsuboi S (1999) Resolving power of surface wave polarization data for higher-order heterogeneities. Geophysical Journal International 138(1):205–220. https://doi.org/10.1046/j.1365-246x.1999.00861.x

Zha Y, Webb SC, Menke W (2013) Determining the orientations of ocean bottom seismometers using ambient noise correlation. Geophysical Research Letters 40(14):3585–3590. https://doi.org/10.1002/grl.50698

Supplementary Material 1 for

Station-orientation catalog for Australian broadband seismic stations

K. Tarumi[1,2*] and K. Yoshizawa[1,2]

[1] Department of Natural History Sciences, Graduate School of Science, Hokkaido University, Sapporo 060-0810, Japan
[2]Department of Earth & Planetary Sciences, Faculty of Science, Hokkaido University, Sapporo 060-0810, Japan.
[*]Corresponding author: tarumi.kotaro.jp@gmail.com

Supplementary Material 1 (this file) includes additional supporting figures (Figures S1-S9) referred to in the main text. The station orientation catalogs for permanent and temporary stations are summarized separately in Supplementary Materials 2 (a separate PDF file), which includes detailed summary tables of our polarization analysis. As demonstrated in the main text, the station orientation depends on the observation period, so we identified the timing of temporal changes by visually checking the time series of P-wave polarization data for each station. The start and end times indicate the initial and final dates for estimating the median angles. Following is a summary of the contents of Supplementary Materials.

- Figures S1–S5: Summary of time-dependent station orientation and the corresponding standard errors. Figures S1 and S2 show the results for permanent stations except for the *S1* network, Figures S3 and S4 for temporary stations, and Figure S5 for the *S1* network.

- Figure S6: An example of three-component P waveforms with or without the correction for horizontal misorientation at the AU.STKA station.

- Figure S7: A map projection of station misorientations from the geographic north for the *S1* network stations.

- Figure S8: Examples of P-wave receiver functions at AU.STKA using the eastern seismic events.

- Figure S9: Examples of P-wave receiver functions at AU.STKA using the western seismic events.

Note that Supplementary Material 2 (another PDF) includes the station orientation catalog (Tables S1–S3).

- Text S1: Description of the *S1* network.

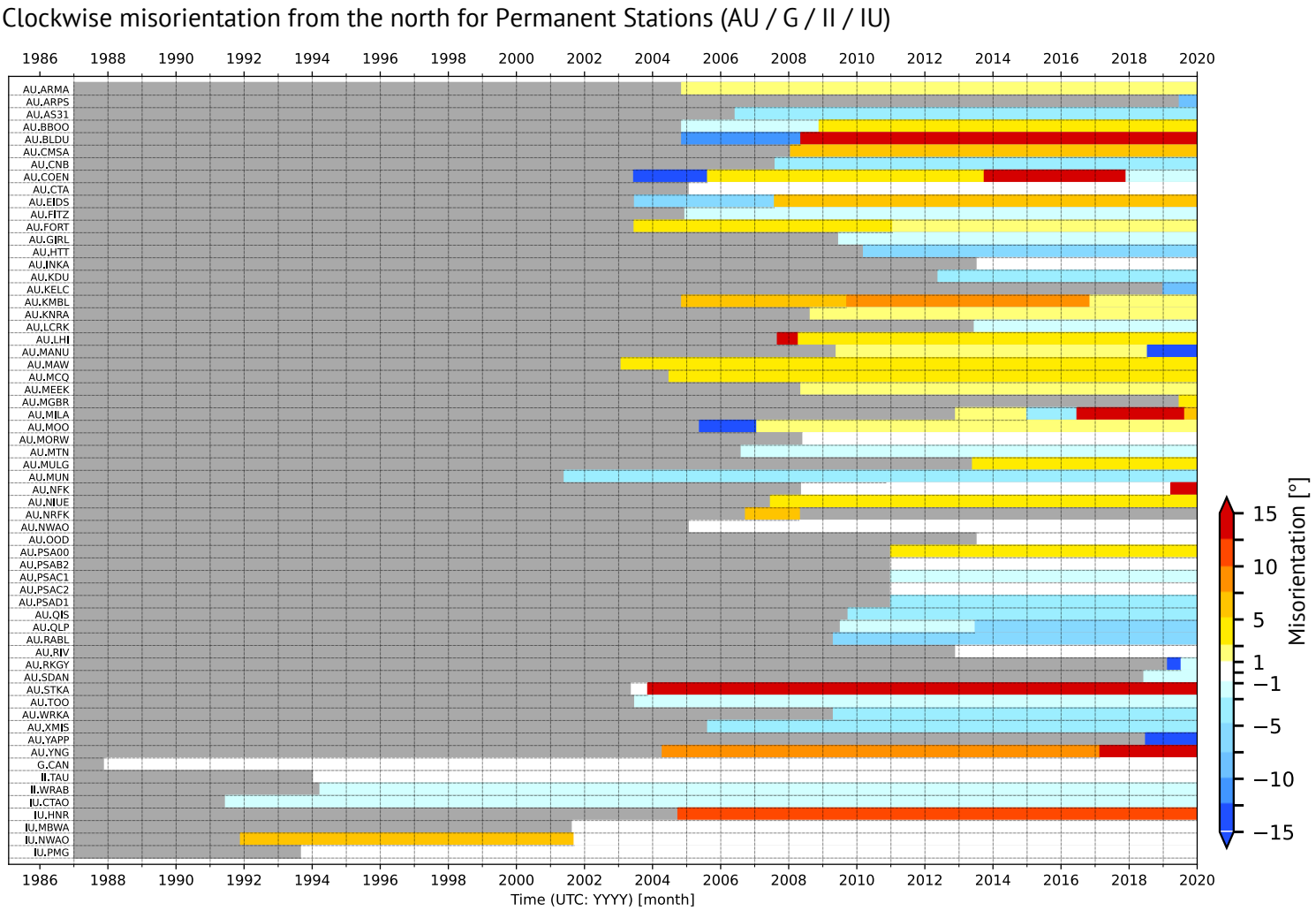

Figure S1. Summary of clockwise misorientation from the geographic north for permanent stations (except for the *S1* network). A positive misorientation value represents the eastward rotation of horizontal sensors from the north. The gray region represents the period when the seismic station was not operational. Note that the operation periods for some stations (AU.ARPS, AU.KELC, AU.MGBR, AU.RKGY, and AU.SDAN) are too short to estimate the proper misorientation in our polarization analysis; see Supplementary Material 2 for details.

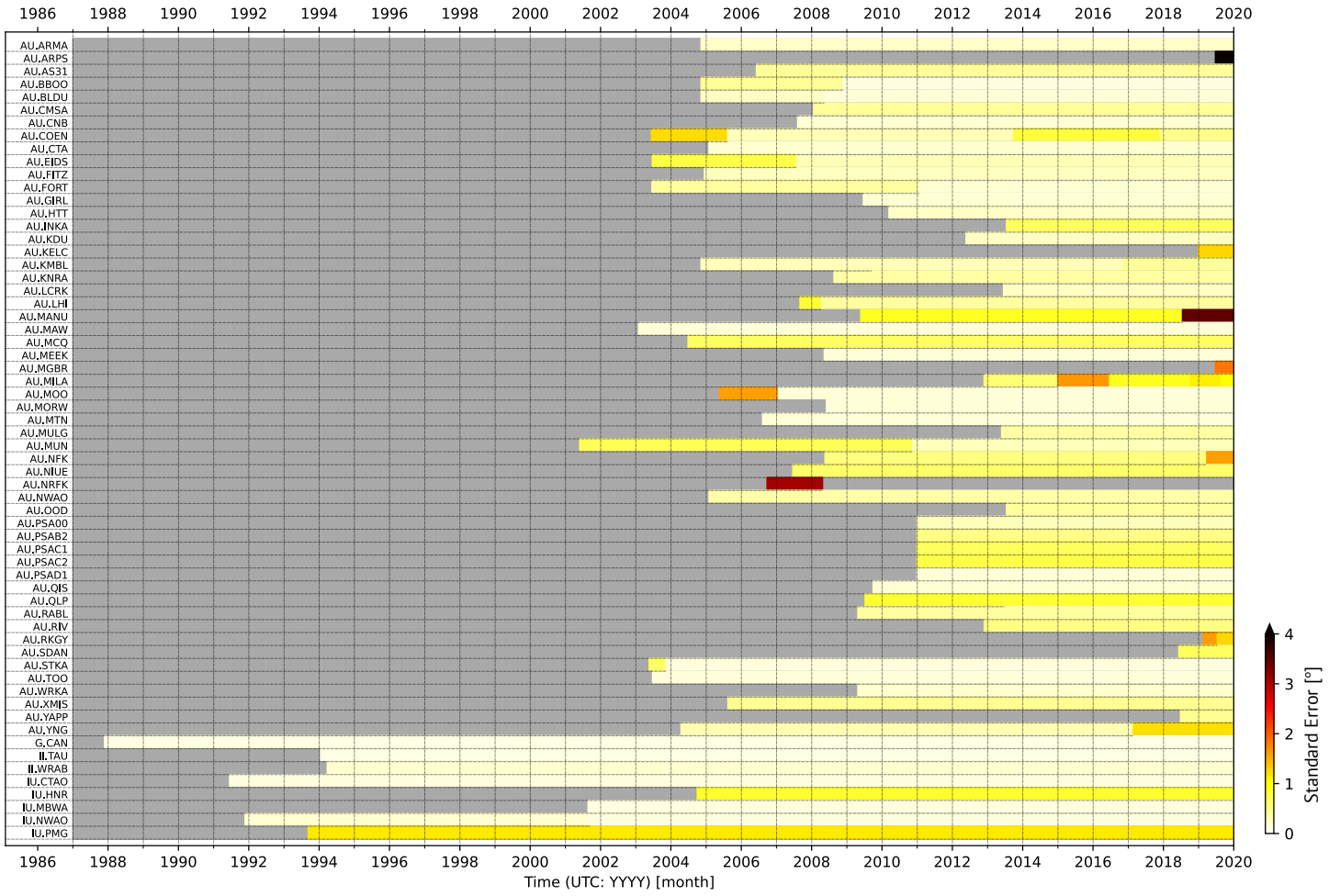

Figure S2. Same as Figure S1, but the summary of standard errors for the estimated misorientation values.

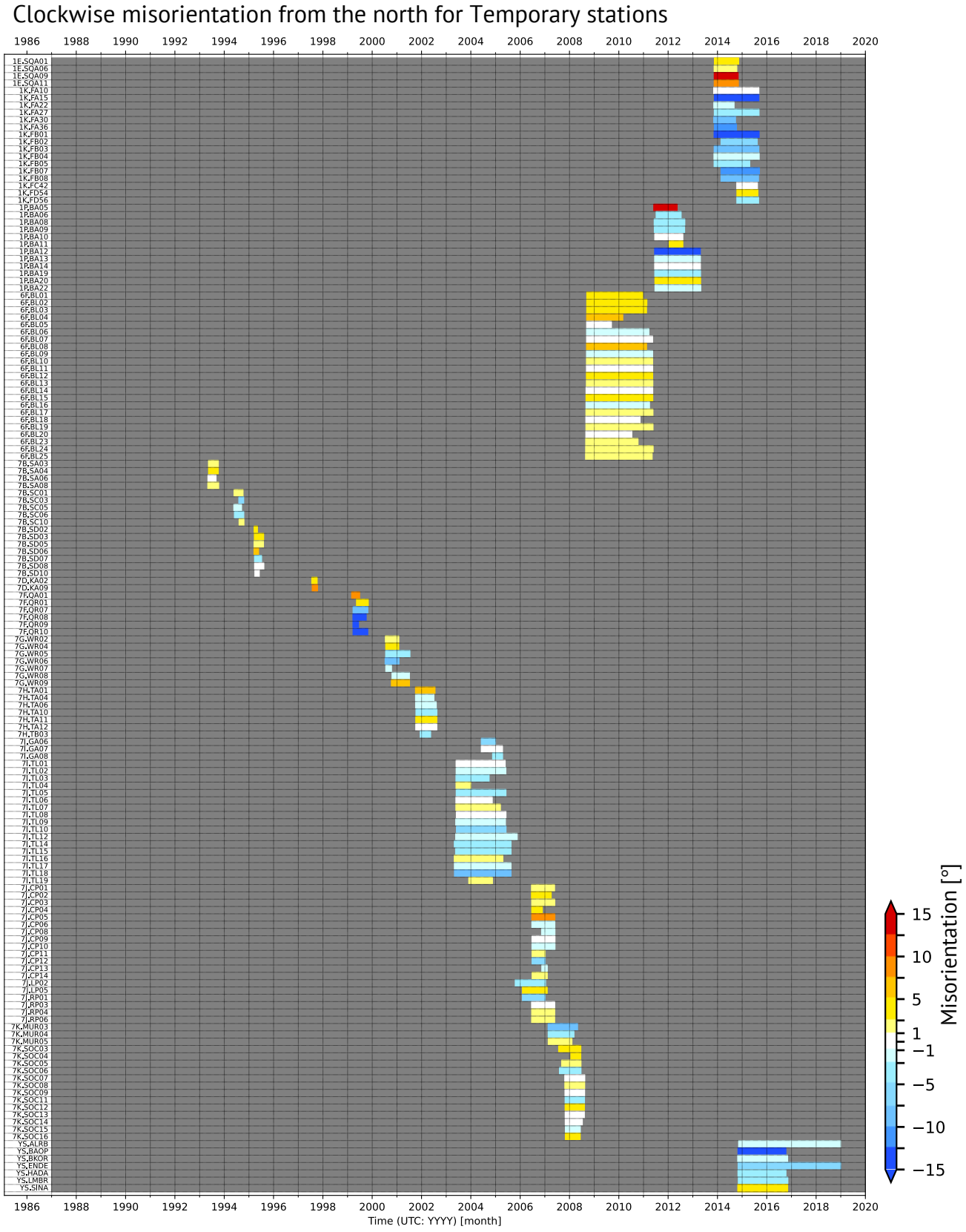

Figure S3: Same as Figure S1, but for the temporary stations.

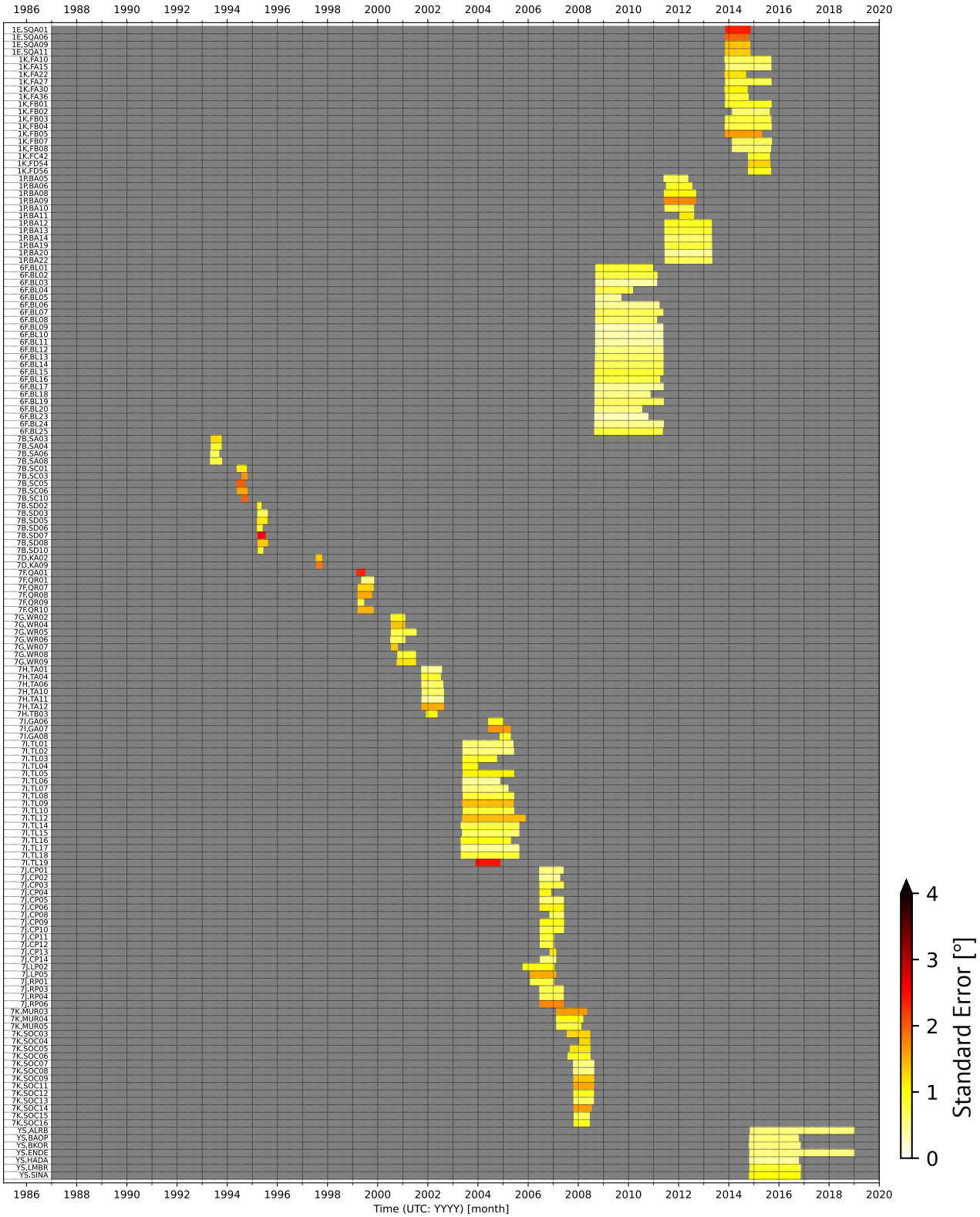

Figure S4: Same as Figure S2, but for the temporary stations.

Summary of S1 Stations

(a) Misorientation

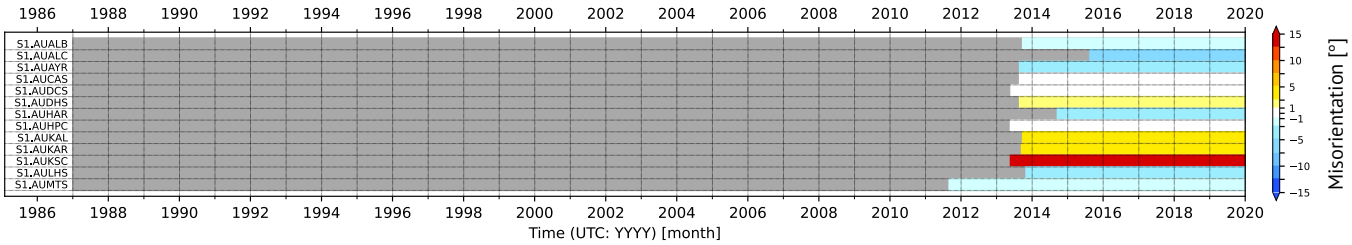

(b) Standard error

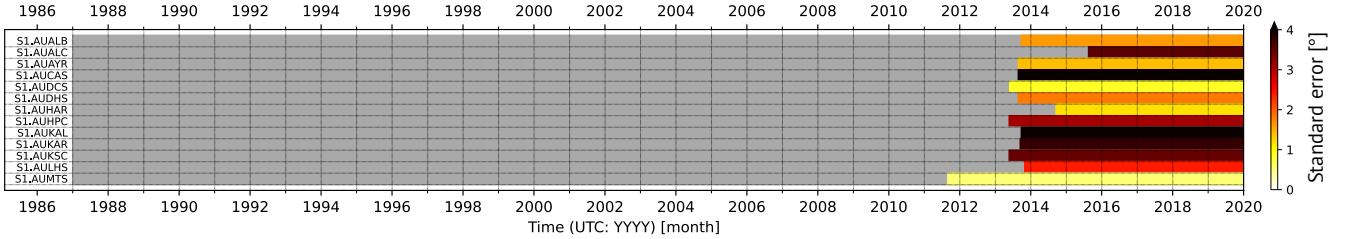

Figure S5: Summary of the *S1* network stations. (a) and (b) are the same as Figures S1 and S2, respectively, but for the *S1* network.

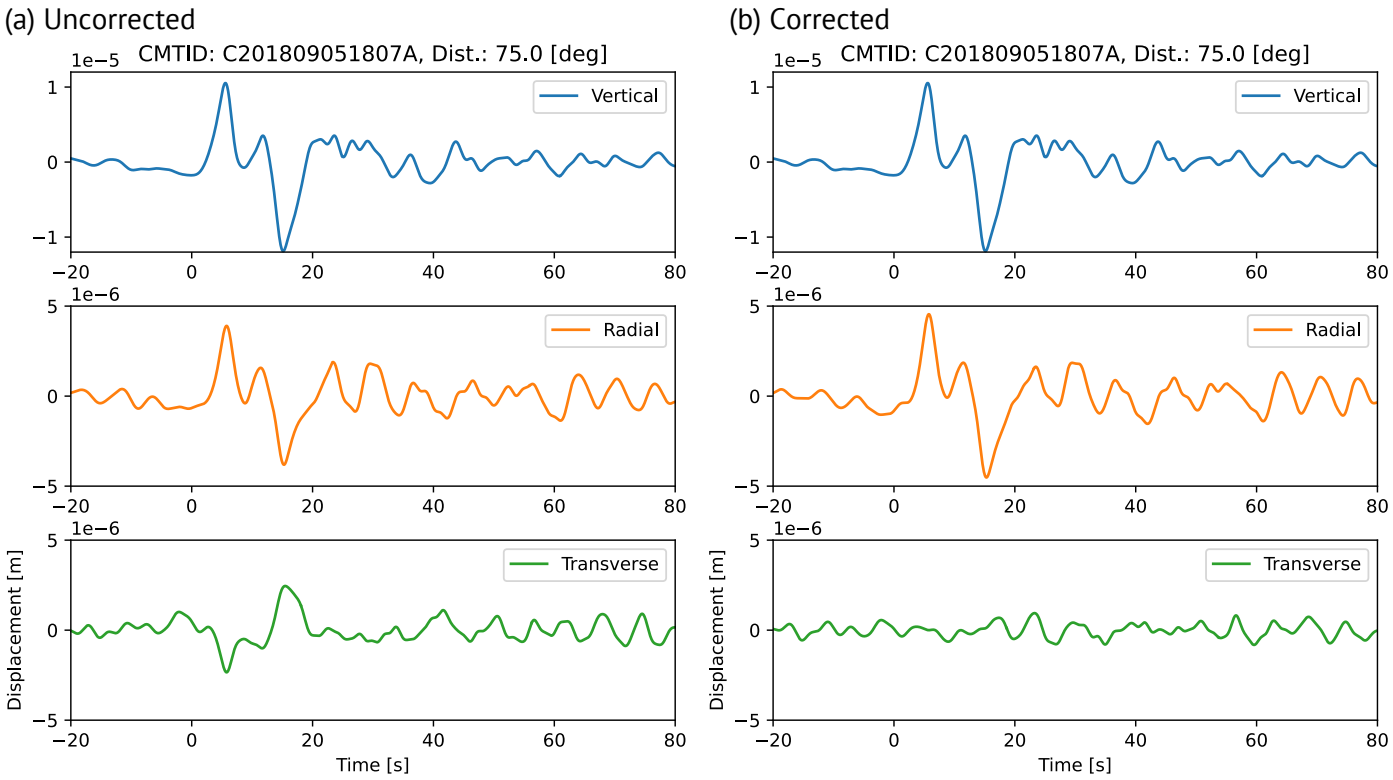

Figure S6: An example of teleseismic P-wave at AU.STKA for a seismic event (Mw 6.6) in Hokkaido, Japan, on September 5, 2018 (UTC). Three-component seismograms (a) before the correction of the station misorientation, and (b) after the correction. Blue, orange, and green lines indicate the vertical, radial, and transverse components. For the uncorrected waveforms in (a), we used the horizontal orientation reported by IRIS/AusPass, while for (b), we employed our new catalog of misorientation. Note that the amplitude scale in the top panel (vertical) is different from the other two horizontal components.

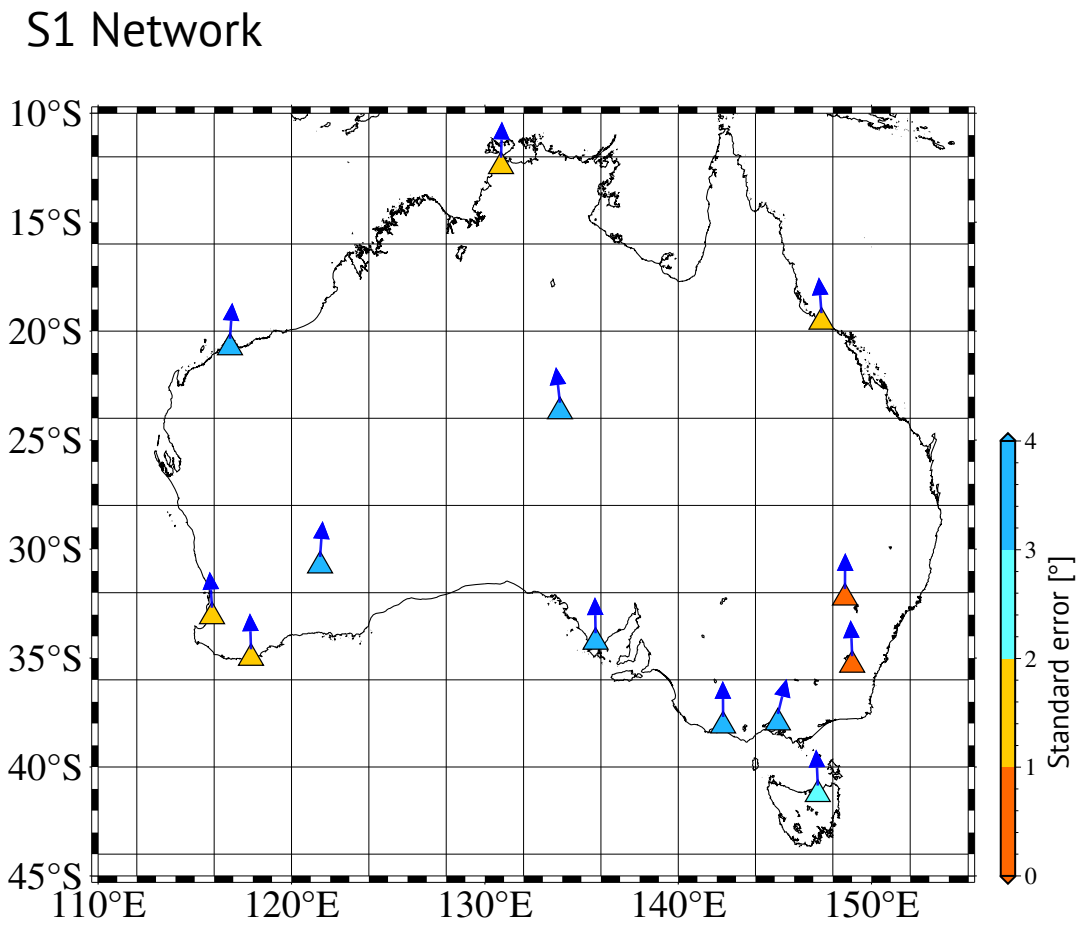

Figure S7: Same as Figures 4 (a-e) and 5 in the main text, but for the *S1* network.

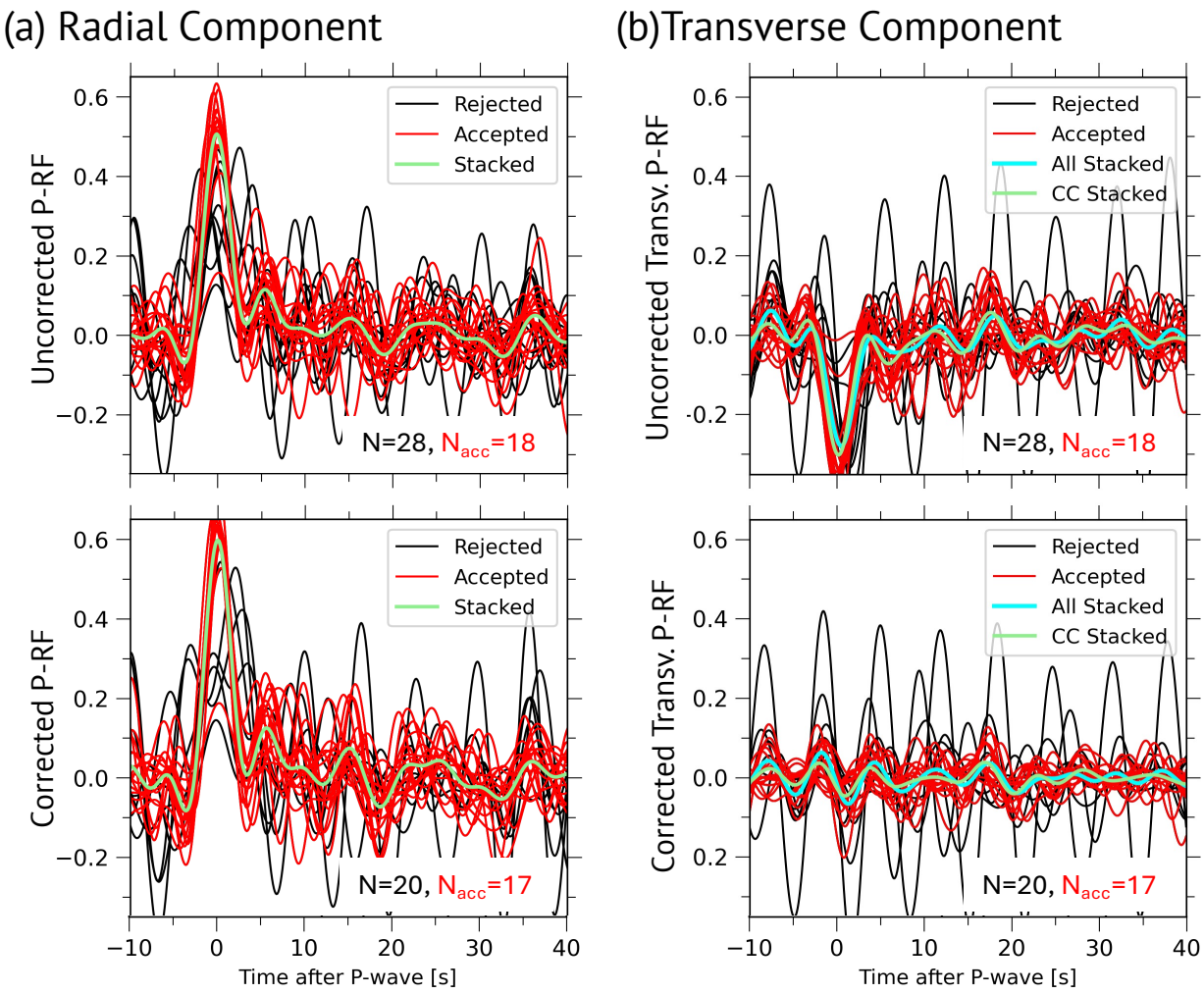

Figure S8: Examples of individual and stacked traces of P-wave receiver functions from the eastern event groups at AU.STKA shown in Figure 5. (a) P-RFs in radial component and (b) transverse component; (top) without and (bottom) with a correction for the station misorientation. Black and red lines are the rejected and accepted traces, respectively, through the cross-correlation-based selection step explained in the main text. Green traces represent the stacked traces, shown as the blue or orange line in Figure 5b.

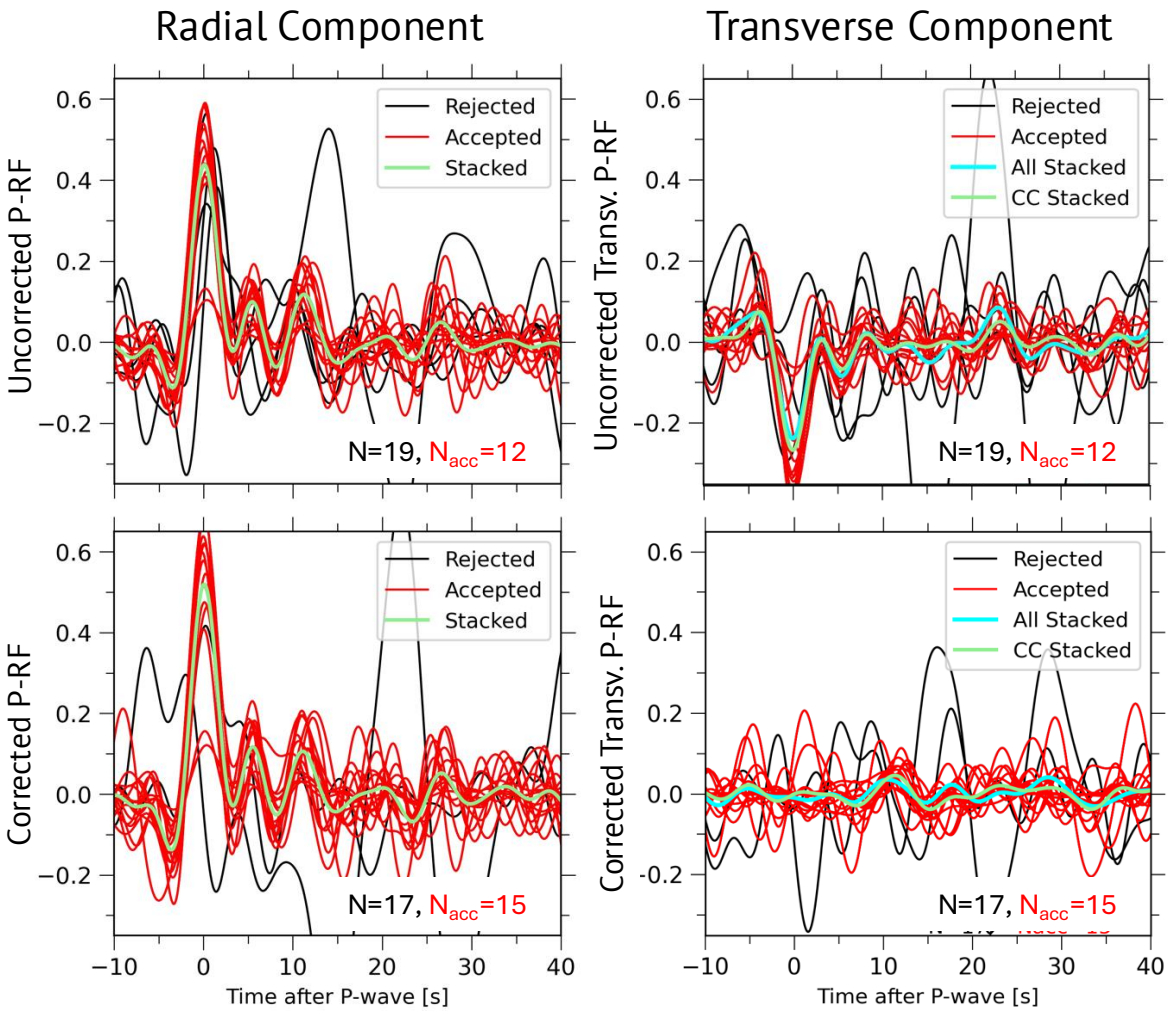

Figure S9: Same as Figure S8, but the P-wave receiver functions from the western event groups.

Text S1: Description of the *S1* network.

Figure S7 shows the map of station orientations for the S1 network (broadband seismometers in schools; Balfour et al., 2014), which has been in operation since 2011 (Salmon et al., 2011). Table S2 in Supplementary Material 2 lists the estimated station orientations and their standard errors.

The seismometers used in the S1 network (Güralp CMG-6TD) (Balfour et al., 2014; Salmon et al., 2011) have a relatively short eigenperiod (30 s) compared to those in other permanent networks used in this study ($\geq$ 120 s, in general). Although we obtained many high-quality arrival-angle measurements when analyzing waveforms in the higher-frequency range (e.g., 0.1–1.0 Hz), we could not collect sufficient measurements to evaluate the station orientation for about half of the S1 stations when focusing on the longer-period range (0.03–0.1 Hz). Consequently, our S1 network catalog (Table S2) includes only 13 stations (Figures S5 and S8).

Balfour, N. J., Salmon, M., & Sambridge, M. (2014). The Australian Seismometers in Schools Network: Education, Outreach, Research, and Monitoring. *Seismological Research Letters*, *85*(5), 1063–1068. https://doi.org/10.1785/0220140025

Salmon, M., Balfour, N., & Sambridge, M. (2011). Australian Seismometers in Schools. AusPass. Retrieved from https://www.fdsn.org/networks/detail/S1/

Supplementary Material 2 for

Station-orientation catalog for Australian broadband seismic stations

K. Tarumi[1,*] and K. Yoshizawa[1,2]

[1] Department of Natural History Sciences, Graduate School of Science, Hokkaido University, Sapporo 060-0810, Japan

[2]Department of Earth & Planetary Sciences, Faculty of Science, Hokkaido University, Sapporo 060-0810, Japan.

[*]Corresponding author: tarumi.kotaro.jp@gmail.com

Supplementary Material 2 (this file) includes additional supporting tables referred to in the main text. Table S1 represents a station orientation catalog for permanent stations except for the *S1* network. Details of tabulated parameters are summarized in the caption in Table S1. Tables S2 and S3 are the same as Table S1 but for the *S1* network and temporary stations, respectively.

Contents of this file:

- Table S1: A Station orientation catalog for permanent stations except for the *S1* network.
- Table S2: A Station orientation catalog for the *S1* network.
- Table S3: A Station orientation catalog for temporary stations.

Table S1: Station orientation catalog for permanent stations except for the *S1* network. The first column includes the network code and station name. The second and third columns represent the period (start and end time) for calculating two statistical values (the median and mean) on station orientation (in the fourth and fifth columns, respectively) and its standard errors from the sixth column. The last column indicates the number of earthquakes used to estimate the misorientation during the designated period.

Network.Station	**Start Time**	**End Time**	**Median [deg]**	**Mean [deg]**	**Std_err [deg]**	N_{ev}
AU.ARMA	2004-11-09T21:48:34.105000Z	2019-12-31T23:59:59.000000Z	2.28	2.55	0.22	588
AU.ARPS	2019-06-25T00:00:00.000000Z	2019-12-31T23:59:59.000000Z	-9.37	-7.47	4.36	6
AU.AS31	2006-06-07T05:38:00.000000Z	2019-12-31T23:59:59.000000Z	-4.35	-5.19	0.42	561
AU.BBOO	2004-11-09T21:48:37.220000Z	2008-11-24T00:00:00.000000Z	-2	-1.45	0.43	159
AU.BBOO	2008-11-24T00:00:00.000000Z	2019-12-31T23:59:59.000000Z	3.62	3.53	0.14	652
AU.BLDU	2004-11-09T21:48:33.800000Z	2008-05-12T00:00:00.000000Z	-11.88	-11.94	0.24	142
AU.BLDU	2008-05-12T00:00:00.000000Z	2019-12-31T23:59:59.000000Z	12.72	11.86	0.16	657
AU.CMSA	2008-01-23T00:00:00.000000Z	2019-12-31T23:59:59.000000Z	5.16	4.02	0.42	508
AU.CNB	2007-08-10T02:32:30.594500Z	2019-12-31T23:59:59.000000Z	-3.55	-3.43	0.18	645
AU.COEN	2003-06-14T00:00:00.000000Z	2005-08-15T00:00:00.000000Z	-17.24	-13.51	1.23	20
AU.COEN	2005-08-15T00:00:00.000000Z	2013-10-01T00:00:00.000000Z	2.62	2.82	0.29	333
AU.COEN	2013-10-01T00:00:00.000000Z	2017-12-01T00:00:00.000000Z	19.97	19.35	0.78	104
AU.COEN	2017-12-01T00:00:00.000000Z	2019-12-31T23:59:59.000000Z	-1.41	-1.73	0.47	81
AU.CTA	2005-01-31T00:00:00.000000Z	2019-12-31T23:59:59.000000Z	0.81	0.87	0.19	538
AU.EIDS	2003-06-23T00:00:00.019500Z	2007-08-03T00:00:00.000000Z	-7.39	-12.19	0.74	130
AU.EIDS	2007-08-03T00:00:00.000000Z	2019-12-31T23:59:59.000000Z	5.09	4.06	0.29	534
AU.FITZ	2004-12-15T00:00:00.000000Z	2019-12-31T23:59:59.000000Z	-2.27	-2.02	0.25	427
AU.FORT	2003-06-19T00:00:00.000000Z	2011-01-23T00:00:00.000000Z	4.36	2.05	0.38	69
AU.FORT	2011-01-23T00:00:00.000000Z	2019-12-31T23:59:59.000000Z	1.37	1.36	0.18	404
AU.GIRL	2009-06-22T00:00:00.000000Z	2019-12-31T23:59:59.000000Z	-1.38	-1.27	0.18	373
AU.HTT	2010-03-15T00:00:00.000000Z	2019-12-31T23:59:59.000000Z	-6.29	-6.61	0.23	399

AU.INKA	2013-07-17T00:00:00.000000Z	2019-12-31T23:59:59.000000Z	0.27	0.29	0.63	37
AU.KDU	2012-05-23T00:00:00.000000Z	2019-12-31T23:59:59.000000Z	-2.57	-2.83	0.24	311
AU.KELC	2019-01-01T00:00:00.000000Z	2019-12-31T23:59:59.000000Z	-9.05	-9.13	1.26	19
AU.KMBL	2004-11-09T21:48:40.360000Z	2009-09-17T00:00:00.000000Z	6.62	6.39	0.28	202
AU.KMBL	2009-09-17T00:00:00.000000Z	2016-11-09T00:00:00.000000Z	7.81	7.71	0.29	203
AU.KMBL	2016-11-09T00:00:00.000000Z	2019-12-31T23:59:59.000000Z	1.28	0.72	0.41	93
AU.KNRA	2008-08-21T00:00:00.000000Z	2019-12-31T23:59:59.000000Z	1.5	0.31	0.37	356
AU.LCRK	2013-06-16T00:00:00.000000Z	2019-12-31T23:59:59.000000Z	-1.57	-2.09	0.24	252
AU.LHI	2007-09-03T04:36:09.594500Z	2008-04-15T00:00:00.000000Z	31.47	29.09	0.81	16
AU.LHI	2008-04-15T00:00:00.000000Z	2019-12-31T23:59:59.000000Z	4.3	4.7	0.39	117
AU.MANU	2009-05-26T00:00:00.000000Z	2018-07-18T00:00:00.000000Z	1.62	2.36	0.89	107
AU.MANU	2018-07-18T00:00:00.000000Z	2019-12-31T23:59:59.000000Z	-27.05	-22.03	3.47	18
AU.MAW	2003-01-31T00:00:00.000000Z	2019-12-31T23:59:59.000000Z	2.89	2.88	0.16	666
AU.MCQ	2004-06-28T00:00:00.000000Z	2019-12-31T23:59:59.000000Z	3.42	3.74	0.64	44
AU.MEEK	2008-05-12T00:00:00.000000Z	2019-12-31T23:59:59.000000Z	2.08	2.22	0.17	574
AU.MGBR	2019-06-24T00:11:23.600000Z	2019-12-31T23:59:59.000000Z	4.37	2.07	1.83	30
AU.MILA	2012-11-27T00:00:00.000000Z	2014-12-31T00:00:00.000000Z	1.68	0.89	0.55	44
AU.MILA	2014-12-31T00:00:00.000000Z	2016-06-22T00:00:00.000000Z	-2.51	-2.04	1.63	22
AU.MILA	2016-06-22T00:00:00.000000Z	2018-10-12T00:00:00.000000Z	82.67	73.93	0.92	18
AU.MILA	2018-10-12T00:00:00.000000Z	2019-08-21T23:59:59.000000Z	16.74	21.25	1.11	17
AU.MILA	2019-08-21T23:59:59.000000Z	2019-12-31T23:59:59.000000Z	6.45	7.7	1.02	12
AU.MOO	2005-05-20T01:36:40.000000Z	2007-01-25T00:00:00.000000Z	-13.84	-20.37	1.58	21
AU.MOO	2007-01-25T00:00:00.000000Z	2019-12-31T23:59:59.000000Z	1.09	0.6	0.16	530
AU.MORW	2008-06-03T00:05:17.594500Z	2019-12-31T23:59:59.000000Z	-0.08	0.35	0.17	665
AU.MTN	2006-08-11T00:00:00.000000Z	2019-12-31T23:59:59.000000Z	-1.09	-0.86	0.16	650
AU.MULG	2013-05-28T00:00:00.000000Z	2019-12-31T23:59:59.000000Z	4.99	4.6	0.36	219
AU.MUN	2001-05-30T00:00:00.000000Z	2010-11-18T00:00:00.000000Z	-2.47	-6.04	0.68	110
AU.MUN	2010-11-18T00:00:00.000000Z	2019-12-31T23:59:59.000000Z	-3.41	-3.55	0.28	424
AU.NFK	2008-05-20T00:00:00.000000Z	2019-03-26T05:26:20.000000Z	0.81	0.45	0.5	150
AU.NFK	2019-03-26T05:26:20.000000Z	2019-12-31T23:59:59.000000Z	40.39	39.78	1.58	9
AU.NIUE	2007-06-21T00:00:00.000000Z	2019-12-31T23:59:59.000000Z	4.02	2.76	0.6	123
AU.NRFK	2006-09-26T00:00:00.000000Z	2008-4-23T00:00:00.000000Z	6.92	17.61	3.08	15

AU.NWAO	2005-01-31T13:00:00.000000Z	2019-12-31T23:59:59.000000Z	-0.07	0.21	0.35	171
AU.OOD	2013-07-17T00:00:00.000000Z	2019-12-31T23:59:59.000000Z	0.99	2.05	0.4	251
AU.PSA00	2011-01-01T00:00:00.000000Z	2019-12-31T23:59:59.000000Z	2.6	3.01	0.28	234
AU.PSAB2	2011-01-01T00:00:00.000000Z	2019-12-31T23:59:59.000000Z	0.8	0.8	0.49	71
AU.PSAC1	2011-01-01T00:00:00.000000Z	2019-12-31T23:59:59.000000Z	-2.29	-2.7	0.65	75
AU.PSAC2	2011-01-01T00:00:00.000000Z	2019-12-31T23:59:59.000000Z	-0.69	-2.17	0.72	45
AU.PSAD1	2011-01-01T00:00:00.000000Z	2019-12-31T23:59:59.000000Z	-3.35	-3.46	0.16	279
AU.QIS	2009-10-01T00:00:00.000000Z	2019-12-31T23:59:59.000000Z	-3.41	-2.56	0.18	447
AU.QLP	2009-07-10T00:00:00.000000Z	2013-06-26T00:00:00.000000Z	-0.99	-0.89	0.81	62
AU.QLP	2013-06-26T00:00:00.000000Z	2019-12-31T23:59:59.000000Z	-5.36	-6.9	0.79	40
AU.RABL	2009-04-26T00:00:00.000000Z	2019-12-31T23:59:59.000000Z	-5.78	-3.72	0.38	271
AU.RIV	2012-11-28T00:00:00.000000Z	2019-12-31T23:59:59.000000Z	0.34	0.3	0.49	76
AU.RKGY	2019-02-19T00:00:00.000000Z	2019-07-15T00:00:00.000000Z	-25.1	-25.28	1.6	9
AU.RKGY	2019-07-15T00:00:00.000000Z	2019-12-31T23:59:59.000000Z	-1.44	-2.78	1.25	16
AU.SDAN	2018-06-10T00:00:00.000000Z	2019-12-31T23:59:59.000000Z	-1.49	-2.34	0.65	48
AU.STKA	2003-05-20T16:41:00.000000Z	2003-11-11T23:59:59.000000Z	-0.14	0.24	0.64	23
AU.STKA	2003-11-11T23:59:59.000000Z	2019-12-31T23:59:59.000000Z	30.98	30.49	0.15	899
AU.TOO	2003-06-25T00:00:00.000000Z	2019-12-31T23:59:59.000000Z	-1.2	-1.76	0.15	658
AU.WRKA	2009-04-26T00:00:00.000000Z	2019-12-31T23:59:59.000000Z	-3.23	-3.33	0.19	542
AU.XMIS	2005-08-16T00:00:00.000000Z	2019-12-31T23:59:59.000000Z	-3.36	-3.63	0.45	166
AU.YAPP	2018-06-27T23:00:32.875000Z	2019-12-31T23:59:59.000000Z	-13	-13.14	0.45	55
AU.YNG	2004-04-16T00:00:00.000000Z	2017-02-23T02:00:00.000000Z	8.73	8.42	0.31	429
AU.YNG	2017-02-23T02:00:00.000000Z	2019-12-31T23:59:59.000000Z	56	48.51	1.21	42
G.CAN	1987-11-27T00:00:00.000000Z	2019-12-31T23:59:59.000000Z	0.58	0.12	0.12	1450
II.TAU	1994-01-17T00:00:00.000000Z	2019-12-31T23:59:59.000000Z	-0.5	-0.45	0.11	1004
II.WRAB	1994-03-27T00:00:00.000000Z	2019-12-31T23:59:59.000000Z	-1.98	-1.38	0.19	954
IU.CTAO	1991-06-17T00:00:00.000000Z	2019-12-31T23:59:59.000000Z	-1.07	-0.72	0.14	1477
IU.HNR	2004-10-01T00:00:00.000000Z	2019-12-31T23:59:59.000000Z	11.24	10.48	0.84	248
IU.MBWA	2001-08-25T00:00:00.000000Z	2019-12-31T23:59:59.000000Z	0.62	0.38	0.14	1051
IU.NWAO	1991-11-25T00:00:00.000000Z	2001-09-13T04:50:00.000000Z	5.82	5.92	0.19	365
IU.NWAO	2001-09-13T04:50:00.000000Z	2019-12-31T23:59:59.000000Z	-0.59	-0.59	0.14	820
IU.PMG	1993-09-10T00:00:00.000000Z	2019-12-31T23:59:59.000000Z	0.09	1.92	1.15	31

Table S2: Same as Table S1, but for the *S1* network stations.

Network.Station	**Start Time**	**End Time**	**Median [deg]**	**Mean [deg]**	**Std_err [deg]**	N_{ev}
S1.AUALB	2013-09-26T00:00:00.000000Z	2019-12-31T23:59:59.000000Z	-1.78	-0.5	1.61	18
S1.AUALC	2015-08-19T00:00:00.000000Z	2019-12-31T23:59:59.000000Z	-6.37	-8.49	3.53	8
S1.AUAYR	2013-08-26T00:00:00.000000Z	2019-12-31T23:59:59.000000Z	-4.21	-6.04	1.4	8
S1.AUCAS	2013-08-26T00:00:00.000000Z	2019-12-31T23:59:59.000000Z	-0.9	4.41	6.81	18
S1.AUDCS	2013-05-30T00:00:00.000000Z	2019-12-31T23:59:59.000000Z	0.27	-4.12	0.87	11
S1.AUDHS	2013-08-26T00:00:00.000000Z	2019-12-31T23:59:59.000000Z	1.61	4.37	1.81	20
S1.AUHAR	2014-09-18T00:00:00.000000Z	2019-12-31T23:59:59.000000Z	-3.63	-7.9	1.2	6
S1.AUHPC	2013-05-24T00:00:00.000000Z	2019-12-31T23:59:59.000000Z	-0.31	2.35	3.09	19
S1.AUKAL	2013-09-26T00:00:00.000000Z	2019-12-31T23:59:59.000000Z	4.07	12.55	12.16	16
S1.AUKAR	2013-09-15T00:00:00.000000Z	2019-12-31T23:59:59.000000Z	3.77	1.77	3.74	5
S1.AUKSC	2013-05-24T00:00:00.000000Z	2019-12-31T23:59:59.000000Z	13.83	10.12	3.44	10
S1.AULHS	2013-10-31T00:00:00.000000Z	2019-12-31T23:59:59.000000Z	-2.56	-6.74	2.39	10
S1.AUMTS	2011-09-01T02:22:00.000000Z	2019-12-31T23:59:59.000000Z	-2.3	-3.65	0.56	26

Table S3: Same as Table S1, but for temporary stations.

Network.Station	Start Time	End Time	Median [deg]	Mean [deg]	Std_err [deg]	N_{ev}
1E.SQA01	2013-11-17T00:58:59.000000Z	2014-11-10T15:22:20.620000Z	3.5	-0.04	2.37	7
1E.SQA06	2013-11-13T03:48:59.000000Z	2014-10-14T05:20:27.020000Z	1.12	1.34	1.93	6
1E.SQA09	2013-11-14T04:42:59.000000Z	2014-11-02T17:29:06.360000Z	15.64	14.97	1.36	7
1E.SQA11	2013-11-14T00:26:59.000000Z	2014-11-06T09:31:39.640000Z	9.19	10.26	1.34	7
1K.FA10	2013-11-06T08:51:59.000000Z	2015-09-05T10:26:37.380000Z	0.05	-1.1	0.68	38
1K.FA15	2013-11-16T23:06:59.000000Z	2015-09-05T16:55:18.660000Z	-13	-12.07	0.54	18
1K.FA22	2013-11-08T06:57:59.000000Z	2014-09-03T11:07:39.340000Z	-2.02	-1.61	1.18	15
1K.FA27	2013-11-15T07:08:59.000000Z	2015-09-08T01:45:32.060000Z	-3.62	-3.88	0.71	30
1K.FA30	2013-11-07T07:40:59.000000Z	2014-09-25T00:36:32.020000Z	-9.47	-10.57	1.09	9
1K.FA36	2013-11-16T03:26:59.000000Z	2014-10-09T00:40:00.140000Z	-11.31	-10.26	0.79	13
1K.FB01	2013-11-12T04:16:59.000000Z	2015-09-09T12:11:27.900000Z	-13.05	-14.37	0.87	24
1K.FB02	2014-02-23T03:35:59.000000Z	2015-08-13T00:23:36.400000Z	-7.5	-7.87	0.59	20
1K.FB03	2013-11-13T08:30:59.000000Z	2015-09-05T03:15:22.140000Z	-8.29	-8.6	0.78	24
1K.FB04	2013-11-10T07:59:59.020000Z	2015-09-10T07:36:17.140000Z	-2.18	-2.36	0.73	24
1K.FB05	2013-11-12T06:46:59.000000Z	2015-04-23T15:33:44.620000Z	-4.86	-1.18	1.6	11
1K.FB07	2014-02-23T08:05:59.000000Z	2015-09-13T13:42:50.660000Z	-11.54	-10.77	0.67	33
1K.FB08	2014-02-23T02:39:59.000000Z	2015-08-31T00:54:58.720000Z	-9.11	-9.41	0.6	34
1K.FC42	2014-10-14T05:09:59.000000Z	2015-08-15T15:13:01.200000Z	-0.74	-1.58	0.87	11
1K.FD54	2014-10-16T04:53:59.000000Z	2015-08-22T10:36:17.020000Z	4.95	4.49	1.28	8
1K.FD56	2014-10-15T07:15:59.000000Z	2015-09-01T15:59:05.800000Z	-4.34	-4.64	0.92	13
1P.BA05	2011-06-02T21:40:59.000000Z	2012-05-13T05:08:45.140000Z	21.05	19.98	0.67	11
1P.BA06	2011-07-08T02:21:59.000000Z	2012-07-11T05:12:47.060000Z	-2.78	-15.38	0.88	6
1P.BA08	2011-06-09T03:44:59.000000Z	2012-09-04T01:17:49.460000Z	-3.55	-3.82	1.03	13
1P.BA09	2011-06-11T04:59:59.000000Z	2012-09-01T05:27:54.260000Z	-4.34	-6.12	1.73	8
1P.BA10	2011-06-17T23:40:57.000000Z	2012-08-06T05:56:48.020000Z	-0.24	1.09	0.7	14
1P.BA11	2012-01-18T03:38:59.000000Z	2012-08-06T03:00:41.300000Z	3.22	2.7	1.13	10
1P.BA12	2011-06-15T06:30:43.000000Z	2013-04-22T03:44:00.980000Z	-36.34	-24.97	0.88	9
1P.BA13	2011-06-16T01:44:59.000000Z	2013-04-22T23:04:00.980000Z	-1.8	-2	0.81	26

1P.BA14	2011-06-16T05:42:59.000000Z	2013-04-23T01:38:00.980000Z	-0.72	-2.47	0.59	23
1P.BA19	2011-06-18T02:15:19.000000Z	2013-04-24T23:08:00.980000Z	-2.68	-3.12	0.75	16
1P.BA20	2011-06-20T02:37:59.000000Z	2013-04-26T02:12:00.980000Z	4.62	3.53	0.43	21
1P.BA22	2011-06-21T01:46:59.000000Z	2013-04-28T01:21:00.980000Z	-1.63	-0.81	0.68	16
6F.BL01	2008-09-14T00:20:59.000000Z	2010-12-20T11:28:00.980000Z	4.35	5.45	0.82	17
6F.BL02	2008-09-13T06:13:59.000000Z	2011-02-20T00:00:00.980000Z	3.2	-0.95	0.74	13
6F.BL03	2008-09-13T01:15:10.000000Z	2011-02-15T07:55:00.960000Z	3.88	4.13	0.35	62
6F.BL04	2008-09-12T05:21:59.000000Z	2010-02-28T10:56:00.980000Z	5.86	7.49	0.73	22
6F.BL05	2008-09-12T00:51:59.000000Z	2009-09-12T23:36:00.980000Z	0.95	0.25	0.4	38
6F.BL06	2008-09-11T01:38:17.000000Z	2011-03-22T02:06:00.980000Z	-1.36	-2.27	0.43	91
6F.BL07	2008-09-11T07:01:02.000000Z	2011-05-16T02:17:00.980000Z	0.64	0.86	0.66	43
6F.BL08	2008-09-10T05:26:59.000000Z	2011-02-15T12:15:00.980000Z	5.86	5.34	0.61	49
6F.BL09	2008-09-10T00:49:26.000000Z	2011-05-16T04:41:00.980000Z	-1.36	-2.72	0.29	88
6F.BL10	2008-09-09T07:10:59.000000Z	2011-05-16T02:07:00.980000Z	1.08	0.42	0.34	82
6F.BL11	2008-09-09T01:26:15.000000Z	2011-05-17T00:51:00.980000Z	0.4	0.06	0.36	125
6F.BL12	2008-09-08T07:58:15.000000Z	2011-05-17T04:40:00.980000Z	2.92	2.42	0.51	59
6F.BL13	2008-09-08T01:33:20.000000Z	2011-05-19T04:35:54.980000Z	1.9	0.4	0.6	76
6F.BL14	2008-09-03T01:11:59.000000Z	2011-05-18T02:45:00.980000Z	-0.69	-1.27	0.67	46
6F.BL15	2008-09-02T09:23:59.000000Z	2011-05-18T07:40:00.980000Z	3.05	2.97	0.8	24
6F.BL16	2008-09-02T01:04:59.000000Z	2011-03-31T04:13:00.980000Z	-1.27	3.29	0.75	26
6F.BL17	2008-09-01T03:51:59.000000Z	2011-05-21T01:03:00.980000Z	1.26	2.3	0.4	62
6F.BL18	2008-08-31T08:40:54.000000Z	2010-11-11T02:04:00.980000Z	-0.26	-2.15	0.48	63
6F.BL19	2008-09-01T00:16:59.000000Z	2011-05-22T00:57:00.980000Z	2.12	0.61	0.64	44
6F.BL20	2008-08-31T01:19:59.000000Z	2010-07-12T03:40:00.980000Z	0.7	0.82	0.52	67
6F.BL23	2008-08-28T23:59:59.000000Z	2010-10-12T00:10:01.980000Z	1.5	9.37	0.27	32
6F.BL24	2008-08-28T02:18:13.000000Z	2011-05-24T00:35:00.980000Z	1.27	0.84	0.45	75
6F.BL25	2008-08-27T03:27:11.000000Z	2011-05-09T03:00:00.980000Z	1.99	1.67	0.77	14
7B.SA03	1993-05-13T01:16:11.857000Z	1993-10-05T03:22:29.526000Z	1.96	3.32	1.22	13
7B.SA04	1993-05-14T06:26:50.846000Z	1993-10-03T22:00:59.799000Z	3.83	0.75	0.8	21
7B.SA06	1993-05-05T00:44:49.846000Z	1993-09-01T00:54:49.800000Z	-0.27	0.36	0.68	10
7B.SA08	1993-05-03T03:00:57.846000Z	1993-10-10T01:30:52.798000Z	1.67	0.94	0.77	6
7B.SC01	1994-05-26T05:45:36.846000Z	1994-10-05T20:48:47.574000Z	1.52	3.93	1.1	18

7B.SC03	1994-08-05T09:40:54.846000Z	1994-10-15T19:20:56.806000Z	-5.74	-5.1	1.63	8
7B.SC05	1994-05-23T05:59:16.381000Z	1994-09-14T06:04:33.250000Z	-1.72	-0.45	1.97	10
7B.SC06	1994-06-01T00:14:07.846000Z	1994-10-17T03:27:48.800000Z	-3.74	-3.78	1.56	10
7B.SC10	1994-08-09T03:59:03.846000Z	1994-10-19T13:59:05.639000Z	2.32	7.54	1.95	6
7B.SD02	1995-03-20T06:17:29.846000Z	1995-05-07T06:37:31.806000Z	3.04	3.4	0.96	10
7B.SD03	1995-03-23T06:11:46.846000Z	1995-08-07T03:08:31.516000Z	2.86	3.37	0.68	14
7B.SD05	1995-03-19T04:34:22.846000Z	1995-08-04T14:27:15.963000Z	1.24	1.5	1.13	8
7B.SD06	1995-03-18T02:38:46.846000Z	1995-05-24T02:28:48.098000Z	5.14	3.92	0.92	12
7B.SD07	1995-03-26T07:49:26.846000Z	1995-07-08T00:00:00.976000Z	-2.88	-3.87	2.5	6
7B.SD08	1995-03-27T09:03:21.842000Z	1995-08-10T01:25:17.015000Z	-0.31	-0.07	1.34	12
7B.SD10	1995-03-31T07:38:35.846000Z	1995-06-03T06:48:39.346000Z	0.34	0.66	0.92	8
7D.KA02	1997-07-21T03:17:09.846000Z	1997-10-07T08:47:12.016000Z	3.33	3.78	1.32	8
7D.KA09	1997-07-27T04:26:09.846000Z	1997-10-13T02:07:21.806000Z	7.98	6.51	1.83	10
7F.QA01	1999-03-04T01:17:40.720000Z	1999-06-29T03:28:32.920000Z	8.7	8.79	2.32	5
7F.QR01	1999-05-14T13:54:18.760000Z	1999-11-04T05:19:10.800000Z	4.85	-2.63	0.5	10
7F.QR07	1999-03-24T07:38:11.840000Z	1999-10-28T05:37:15.600000Z	-8.69	-8.79	1.27	7
7F.QR08	1999-03-22T04:06:11.840000Z	1999-10-04T05:06:19.480000Z	-13.36	-13.39	1.53	8
7F.QR09	1999-03-22T23:54:37.840000Z	1999-06-12T03:26:16.040000Z	-13.19	-13.47	0.76	6
7F.QR10	1999-03-24T00:54:45.400000Z	1999-10-27T10:25:02.520000Z	-17.63	-16.92	1.46	8
7G.WR02	2000-07-15T04:17:48.720000Z	2001-01-29T07:33:21.815300Z	2.24	2.04	0.9	12
7G.WR04	2000-07-20T04:04:12.712300Z	2001-01-28T03:34:21.465200Z	2.49	3.09	1.36	14
7G.WR05	2000-07-19T02:25:43.720000Z	2001-07-13T02:32:14.820100Z	-3.36	-2.33	0.74	27
7G.WR06	2000-07-11T04:19:57.720000Z	2001-01-31T07:49:11.102700Z	-8.36	-8.05	0.67	30
7G.WR07	2000-07-21T06:29:08.720000Z	2000-10-13T02:01:40.299400Z	-2.23	-1.24	1.33	10
7G.WR08	2000-10-21T06:32:29.719900Z	2001-07-05T03:07:43.343900Z	-1.6	-1.03	0.81	21
7G.WR09	2000-10-12T02:53:58.720000Z	2001-07-06T04:57:10.175800Z	6.39	4.86	1.17	24
7H.TA01	2001-10-04T03:19:27.840000Z	2002-07-18T21:22:44.200000Z	6.49	6.93	0.43	6
7H.TA04	2001-10-05T01:46:50.720000Z	2002-07-03T00:37:34.720000Z	-1.45	0.4	0.85	10
7H.TA06	2001-10-06T01:14:39.720000Z	2002-08-07T01:04:29.440000Z	-1.29	-3.63	0.61	7
7H.TA10	2001-10-11T00:36:33.720000Z	2002-08-16T00:54:24.520000Z	-3.13	0.72	0.64	11
7H.TA11	2001-10-08T04:35:41.720000Z	2002-08-15T01:58:40.040000Z	4.13	5.37	0.38	10
7H.TA12	2001-10-07T23:30:51.720000Z	2002-08-15T00:18:47.280000Z	0.31	-4.39	1.51	8

7H.TB03	2001-12-13T00:03:48.840000Z	2002-05-15T08:12:10.560000Z	-3.27	-2.53	1.02	8
7I.GA06	2004-06-05T01:25:40.520000Z	2004-12-31T23:57:33.800000Z	-6.3	-4.36	0.94	9
7I.GA07	2004-06-05T06:09:39.840000Z	2005-04-14T00:48:40.800000Z	-0.91	-1.66	1.64	8
7I.GA08	2004-11-19T02:02:38.880000Z	2005-04-14T23:33:46.440000Z	-3.41	-4.69	0.87	10
7I.TL01	2003-05-28T04:37:01.680000Z	2005-05-23T11:37:32.240000Z	-0.19	0.21	0.57	29
7I.TL02	2003-05-29T03:00:28.680000Z	2005-06-02T03:48:31.640000Z	-1.33	0.25	0.51	31
7I.TL03	2003-05-26T05:31:03.680000Z	2004-09-27T04:30:17.800000Z	-4.14	-4.58	0.85	13
7I.TL04	2003-05-27T03:51:59.000000Z	2004-01-01T00:00:00.960000Z	1.44	-0.08	0.96	15
7I.TL05	2003-05-30T02:28:59.000000Z	2005-06-04T01:28:54.720000Z	-3.84	-3.85	1.09	6
7I.TL06	2003-05-25T07:28:59.000000Z	2004-11-13T03:44:22.080000Z	-0.67	-0.9	0.38	57
7I.TL07	2003-05-25T02:21:59.000000Z	2005-03-14T08:00:00.960000Z	1.26	2.96	0.52	41
7I.TL08	2003-06-01T02:59:59.000000Z	2005-06-04T02:09:25.440000Z	0.47	-0.53	0.78	16
7I.TL09	2003-05-23T03:19:59.000000Z	2005-05-27T03:25:33.120000Z	-0.95	10.82	1.42	8
7I.TL10	2003-06-02T01:09:34.720000Z	2005-06-05T00:00:39.080000Z	-6.1	-4.76	0.76	19
7I.TL12	2003-05-22T07:16:59.000000Z	2005-11-17T05:02:42.240000Z	-2.25	1.43	1.42	23
7I.TL14	2003-05-02T02:59:59.000000Z	2005-08-18T00:00:00.960000Z	-4.37	-4.05	0.72	38
7I.TL15	2003-05-21T00:27:59.000000Z	2005-08-18T00:00:00.960000Z	-3.83	-3.46	0.59	26
7I.TL16	2003-05-01T00:29:59.000000Z	2005-04-19T03:09:25.440000Z	2.4	0.86	0.94	18
7I.TL17	2003-05-03T03:27:59.000000Z	2005-08-18T00:00:00.960000Z	-1.42	-1.07	0.4	30
7I.TL18	2003-05-04T01:25:00.840000Z	2005-08-17T23:00:00.960000Z	-7.62	-7.39	0.75	43
7I.TL19	2003-12-02T03:45:59.000000Z	2004-11-16T03:02:42.240000Z	1.68	2.36	2.43	7
7J.CP01	2006-06-18T08:23:52.000000Z	2007-05-25T00:00:00.960000Z	1.28	1.04	0.51	40
7J.CP02	2006-06-18T04:36:59.000000Z	2007-04-05T02:00:00.960000Z	3.91	1.96	0.42	21
7J.CP03	2006-06-21T07:49:29.000000Z	2007-05-28T00:00:00.960000Z	1.84	0.68	0.77	17
7J.CP04	2006-06-22T01:38:46.000000Z	2006-11-24T06:57:00.960000Z	4.85	4.74	1.06	20
7J.CP05	2006-06-22T06:26:59.000000Z	2007-05-29T00:00:00.960000Z	8.3	7.67	0.56	30
7J.CP06	2006-06-23T07:14:28.000000Z	2007-05-29T00:00:00.960000Z	-2.26	-2.19	1.07	22
7J.CP08	2006-11-14T23:59:59.000000Z	2007-05-30T06:27:00.960000Z	-1.18	-2.81	0.63	20
7J.CP09	2006-06-25T07:01:59.000000Z	2007-05-31T00:00:00.960000Z	1	-0.31	0.96	15
7J.CP10	2006-06-25T02:51:59.000000Z	2007-05-31T00:00:00.960000Z	-1.13	0.54	0.71	25
7J.CP11	2006-06-26T03:59:59.000000Z	2007-01-06T00:00:00.960000Z	1.21	-0.93	0.77	20
7J.CP12	2006-06-26T06:36:20.000000Z	2007-01-06T00:00:00.960000Z	-4.93	-4.04	0.74	19

7J.CP13	2006-11-17T23:59:59.000000Z	2007-02-06T00:00:00.960000Z	-2.02	-2.04	1.11	11
7J.CP14	2006-06-27T07:33:59.000000Z	2007-02-06T00:00:00.960000Z	1.24	1.44	0.52	34
7J.LP02	2005-10-20T02:44:30.846000Z	2007-01-11T12:21:47.844000Z	-2.88	-3.25	0.99	12
7J.LP05	2006-02-04T07:22:13.846000Z	2007-02-05T00:00:00.966000Z	4.17	2.63	1.53	14
7J.RP01	2006-02-04T03:12:14.846000Z	2007-01-05T00:00:00.966000Z	-6.84	-5.71	0.78	13
7J.RP03	2006-06-19T03:26:17.000000Z	2007-05-27T00:00:00.960000Z	0.91	-2.75	0.71	15
7J.RP04	2006-06-21T01:28:59.000000Z	2007-05-27T00:00:00.960000Z	1.64	6.19	0.69	18
7J.RP06	2006-06-20T07:46:59.000000Z	2007-05-26T00:00:00.960000Z	2.38	2.35	1.73	10
7K.MUR03	2007-02-19T01:06:05.718100Z	2008-04-29T18:05:59.998500Z	-8.29	-7.82	1.6	7
7K.MUR04	2007-02-20T00:40:11.718000Z	2008-03-07T00:00:01.935400Z	-3.91	-1.98	0.92	9
7K.MUR05	2007-02-21T06:35:16.718000Z	2008-02-06T00:00:01.669100Z	2.4	0.16	0.75	10
7K.SOC03	2007-07-25T06:57:39.720000Z	2008-06-16T23:18:17.921200Z	2.71	2.5	1.26	6
7K.SOC04	2008-01-21T22:48:59.000000Z	2008-06-16T00:00:00.960000Z	4.9	5.28	1.25	13
7K.SOC05	2007-09-07T23:59:59.000000Z	2008-06-18T23:55:47.520000Z	1.92	1.14	1.15	7
7K.SOC06	2007-08-06T03:05:59.000000Z	2008-06-19T05:22:51.840000Z	-2.57	-2	0.85	28
7K.SOC07	2007-10-24T02:08:59.000000Z	2008-08-14T03:53:46.560000Z	0.15	-0.2	0.5	19
7K.SOC08	2007-10-25T03:27:59.000000Z	2008-08-13T00:00:00.960000Z	1.97	0.5	0.46	33
7K.SOC09	2007-10-27T03:02:59.000000Z	2008-08-12T01:22:51.840000Z	-0.08	-0.36	1.32	12
7K.SOC11	2007-10-28T23:59:59.000000Z	2008-08-10T00:50:24.960000Z	-2.53	-8.75	1.54	9
7K.SOC12	2007-10-29T02:46:59.000000Z	2008-08-09T02:02:42.240000Z	3.85	3.43	0.9	15
7K.SOC13	2007-10-30T03:37:53.000000Z	2008-08-08T00:00:00.960000Z	0.96	1.96	0.65	29
7K.SOC14	2007-10-31T02:28:59.000000Z	2008-07-09T00:00:00.960000Z	0.74	1.91	1.58	8
7K.SOC15	2007-11-01T23:59:59.000000Z	2008-06-09T00:00:00.960000Z	-1.54	-3.13	0.7	36
7K.SOC16	2007-11-01T08:01:59.000000Z	2008-06-08T00:00:00.960000Z	2.62	2.4	0.92	22
YS.ALRB	2014-11-11T07:26:54.380000Z	2018-12-31T23:59:59.000000Z	-2.35	-1.49	0.53	41
YS.BAOP	2014-11-01T00:00:00.000000Z	2016-10-10T07:26:09.200000Z	-14.02	-14.08	0.53	42
YS.BKOR	2014-10-28T04:59:59.200000Z	2016-11-05T02:13:03.180001Z	-1.66	-8.03	0.53	55
YS.ENDE	2014-11-03T05:33:32.200000Z	2018-12-31T23:59:59.000000Z	-6.36	-6.91	0.52	42
YS.HADA	2014-11-01T04:13:50.200000Z	2016-10-11T00:05:59.180001Z	-3.8	-3.7	0.4	105
YS.LMBR	2014-11-06T07:41:25.200000Z	2016-11-08T02:36:46.180001Z	-3.37	8.93	0.83	10
YS.SINA	2014-10-29T07:03:10.200000Z	2016-11-05T06:47:01.180001Z	3.18	4.92	1.01	39